Geophysical Journal International

Geophys. J. Int. (2022) **228,** 551–588
Advance Access publication 2021 September 03
GJI Seismology

https://doi.org/10.1093/gji/ggab357

Seismic waves in medium with poroelastic/elastic interfaces: a two-dimensional *P-SV* finite-difference modelling

David Gregor [1], Peter Moczo [1,2], Jozef Kristek [1,2], Arnaud Mesgouez,[3] Gaëlle Lefeuve-Mesgouez,[3] Christina Morency,[4] Julien Diaz[5] and Miriam Kristekova [1,2]

[1] *Faculty of Mathematics, Physics and Informatics, Comenius University Bratislava, Mlynska dolina F*1, 84248 *Bratislava, Slovak Republic.*
E-mail: moczo@fmph.uniba.sk
[2] *Earth Science Institute, Slovak Academy of Sciences, Dubravska cesta* 9, 84528 *Bratislava, Slovak Republic*
[3] *Avignon Université, INRAE, UMR EMMAH, BP*21239, *F*-84911 *Avignon, France*
[4] *Atmospheric, Earth, and Energy Division, Lawrence Livermore National Laboratory, Livermore, CA* 94551, *USA*
[5] *INRIA, Université de Pau et des Pays de l'Adour, BP* 1155, 64013 *Pau Cedex, France*

Accepted 2021 September 1. Received 2021 August 20; in original form 2020 December 8

SUMMARY

We present a new methodology of the finite-difference (FD) modelling of seismic wave propagation in a strongly heterogeneous medium composed of poroelastic (P) and (strictly) elastic (E) parts. The medium can include P/P, P/E and E/E material interfaces of arbitrary shapes. The poroelastic part can be with (i) zero resistive friction, (ii) non-zero constant resistive friction or (iii) JKD model of the frequency-dependent permeability and resistive friction. Our FD scheme is capable of subcell resolution: a material interface can have an arbitrary position in the spatial grid. The scheme keeps computational efficiency of the scheme for a smoothly and weakly heterogeneous medium (medium without material interfaces). Numerical tests against independent analytical, semi-analytical and spectral-element methods prove the efficiency and accuracy of our FD modelling. In numerical examples, we indicate effect of the P/E interfaces for the poroelastic medium with a constant resistive friction and medium with the JKD model of the frequency-dependent permeability and resistive friction. We address the 2-D *P-SV* problem. The approach can be readily extended to the 3-D problem.

Key words: Permeability and porosity; Numerical approximations and analysis; Computational seismology; Earthquake ground motions; Theoretical seismology; Wave propagation.

1 INTRODUCTION

Real surface or near-surface Earth structures are complex due to their rheological and geometrical properties. They consist of viscoelastic sediments, porous rocks and fluids, often in complex geometrical configurations. Consequently, wave propagation coupling in structures with acoustic/poroelastic, elastic/poroelastic and solid/fluid interfaces has been intensively investigated in the exploration/reservoir geophysics and ocean acoustics.

Laterally fully or partially bounded sediments in surface sedimentary basins and valleys are well known for their potential to cause anomalous earthquake ground motion. Such anomalous motion is often responsible for largest damage in earthquakes.

Earthquake ground motion in surface sedimentary structures can be significantly affected by geometry of the sediment/basement interface, velocity and impedance contrast at the interface, and rheology of sediments (e.g. Kristek *et al.* 2018; Moczo *et al.* 2018). Effects of water- and air-saturated sediments in surface sedimentary basins and valleys on earthquake ground motion in the earthquake engineering frequency range (approximately 0–25 Hz) has not been sufficiently investigated yet. Géli *et al.* (1987) investigated seismic wave propagation in a very permeable water-saturated horizontal surface layer over an elastic half-space. Wuttke *et al.* (2017) investigated motion in surface canyon and elastic inclusion in the poroelastic half-space.

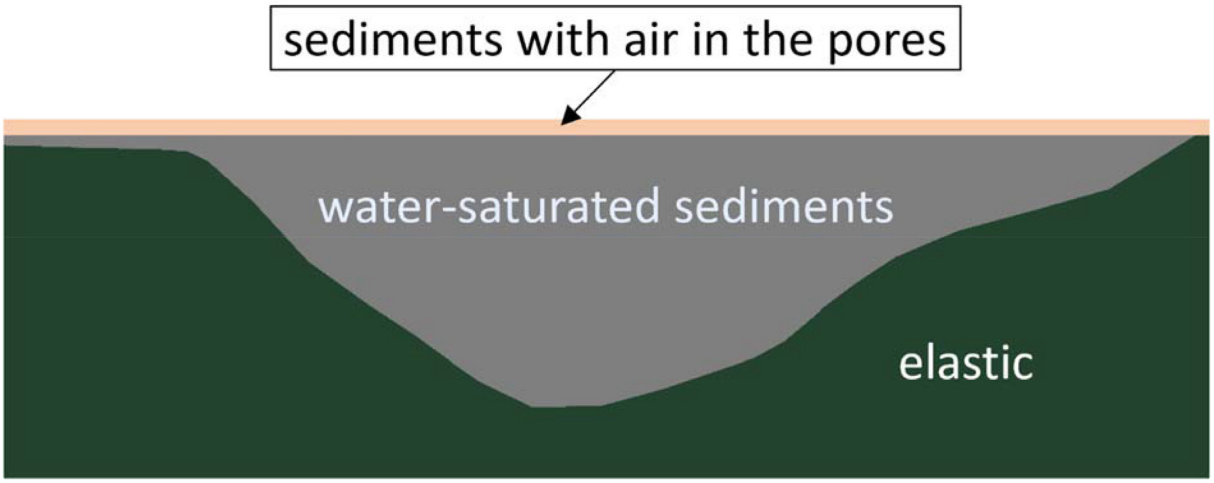

Figure 1. Model of a surface sedimentary basin with an elastic bedrock, water-saturated sediments and surficial thin layer of sediments with air in the pores.

Investigations of effects of poroelasticity on earthquake ground motion in geometrically realistic configurations require sufficiently accurate and computationally efficient numerical methods. Obviously, it would be desirable to have a numerical scheme capable of modelling seismic waves in realistic models consisting of viscoelastic solids, poroviscoelastic rocks and fluids.

1.1 Our goal

Due to relative mathematical and algorithmic complexity, it is reasonable to develop first a finite-difference (FD) scheme capable to simulate seismic waves in strongly heterogeneous models consisting of the poroelastic and elastic parts and thus including poroelastic/elastic (P/E) interfaces. Once the methodology for the model consisting of the poroelastic and elastic parts is developed, its generalization to a model consisting of poroviscoelastic parts and viscoelastic parts should be more feasible in the follow-up paper. Moreover, it is necessary to have the poroelastic/elastic modelling developed for testing and for comparison with the poroviscoelastic/viscoelastic modelling.

Often in the published papers, an elastic part is modelled as a poroelastic part: poroelastic parameters are tuned so that the poroelastic medium effectively behaves as the elastic medium. However, this approach has its limitations: it is not always possible to replace an elastic medium by a suitable poroelastic one.

This means that it is reasonable to develop a scheme for a poroelastic medium that can be used also for the model of medium consisting of both the poroelastic parts and strictly elastic parts. This is methodologically an obvious aspect and goal. It will be good to have such a scheme available for simulating seismic waves in models for which the use of one poroelastic schemes is computationally efficient.

If a major part of the model is elastic and the poroelastic part is relatively small, then the computationally more demanding poroelastic scheme applied to the whole model will be less computationally efficient than, for example, application of the elastic scheme to the elastic part and the poroelastic scheme to the poroelastic part. The use of one scheme or combination of two schemes should be considered specifically for each model and possibly spatial grid (uniform, discontinuous and adaptive).

Our goal here is to develop methodology and an FD scheme with the sub-cell resolution capability in the strongly heterogeneous medium consisting of the poroelastic and elastic parts. An illustrative example is shown in Fig. 1. We address the 2-D *P-SV* problem. The approach can be readily extended to the 3-D problem.

1.2 Previous investigations

Moczo *et al.* (2019) presented a relatively detailed overview of the FD modelling of seismic wave propagation in the poroeleastic medium. Therefore, here we just briefly comment contributions relevant to the specific topic of this paper and recent important contributions which were not mentioned in the above paper.

The problem of the poroelastic/elastic interface and the relation between poroelastic and elastic behaviours was addressed by many authors. Boundary conditions between two poroelastic media, elastic and poroelastic media, and liquid and poroelastic media were found by Deresiewicz & Skalak (1963) who investigated conditions for ensuring uniqueness of solution within framework of Biot's (1956) theory. Alternative independent methodological approaches were used by Lovera (1987) and de la Cruz & Spanos (1989) who derived boundary conditions at the three types of interface.

Géli *et al.* (1987) investigated seismic wave propagation and amplification of earthquake ground motion in a very permeable water-saturated horizontal surface layer over an elastic half-space.

Tomar & Arora (2006) studied reflection and transmission of incident waves at a plane surface between an unsaturated porous half-space and an elastic solid half-space.

Coupling between the elastic and poroelastic media was addressed by Morency & Tromp (2008) in their spectral-element (SE) approach. They accommodated first-order interfaces using domain decomposition. Morency *et al.* (2011) investigated seismic wavefield in a model of a brine-saturated aquifer (poroelastic) sandwiched between elastic layers.

Guan & Hu (2011) developed a 2-D velocity-stress-pressure FD scheme on a staggered grid for simulating elastic waves in medium consisting of elastic, fluid and poroelastic parts. A constant resistive friction is assumed in the poroelastic medium. The scheme is based on modified Biot's equations used to describe wave propagation in the elastic, fluid and poroelastic media, and parameter averaging at material interfaces located along contacts of homogeneous grid cells.

Chen *et al.* (2012) investigated propagation of plane *P* waves at an interface between elastic solid and unsaturated poroelastic medium using analytical method. Lähivaara *et al.* (2014, 2015) investigated possibility to replace a poroelastic aquifer by a highly approximate elastic model. Ward *et al.* (2017, 2020) developed a high-order discontinuous Galerkin method for modelling wave propagation in coupled poroelastic–elastic media in 2-D and 3-D cases, respectively. They derived an upwind numerical flux as an exact solution for the Riemann problem including the poroelastic–elastic interface. Zhang *et al.* (2019) developed an arbitrary high-order discontinuous Galerkin method to simulate the wave propagation in coupled elastic–poroelastic media, which achieves the same order accuracy in time and space domains simultaneously. The interfaces between the two media are explicitly tackled by the Godunov numerical flux.

New recent contributions to the numerical modelling of seismic waves in poroelastic media include the following papers. Sun *et al.* (2019) developed 2-D poroelastic wave modelling with a topographic free surface by the curvilinear grid FD collocated-grid method. Ou & Wang (2019) used the FDTD (FD time-domain) modelling to investigate Stoneley wave reflection from a porous formation in the borehole. He *et al.* (2020) derived boundary conditions at the elastic–poroelastic interface inside the perfectly matched layer (PML) in the unsplit formulation. They also presented a weak form of the PML formulations for the coupled poroelastic problems. Zhang (2020) developed an analysis of stability of high-order FD staggered-grid scheme for 3-D wave propagation in the poroelastic medium and obtained explicit condition for the time step. Considering equations for 3-D wave propagation in the elastic medium as the limit case of those for the poroelastic medium, Zhang easily obtained explicit stability conditions also for the scheme for the elastic medium. He *et al.* (2021) developed a Runge–Kutta discontinuous Galerkin (RKDG) method for solving wave equations in isotropic and anisotropic poroelastic media at low frequencies. Alkhimenkov *et al.* (2021a) developed a comprehensive von Neumann stability analysis for a class of FD schemes for Biot's equations for a poroelastic medium. Alkhimenkov *et al.* (2021b) developed a multi-GPU solver for the anisotropic elastodynamic Biot's equations in 1-D, 2-D and 3-D. They implemented a simple approach to circumvent the stiffness of Biot's equations by using an implicit scheme for Darcy's flux while keeping explicit updates in the iteration loop. Tohti *et al.* (2021) presented the staggered-grid FD microseismic forward modelling in orthorhombic poroelastic medium for an isotropic, double-couple and compensated linear vector dipole sources. Cheng *et al.* (2021) extended the Biot's squirt model to the orthorhombic anisotropy, introduced rheology of the generalized Zener body in the solid matrix and simulated seismic wavefields using the staggered-grid FD scheme.

1.3 FD modelling with subcell resolution capability

Moczo *et al.* (2019) and Gregor *et al.* (2021) developed a discrete representation of a strongly heterogeneous poroelastic medium, that is medium with material interfaces, and the corresponding FD scheme. The averaging was developed for the velocity–stress–pressure staggered-grid scheme with the second-order accuracy in time and fourth-order accuracy in space.

Their scheme has several important features. It can simulate seismic waves in a strongly heterogeneous poroelastic medium with zero resistive friction or non-zero constant resistive friction or JKD model of the frequency-dependent permeability and resistive friction. The scheme has the subcell resolution capability. Due to the decision on compromise between accuracy and computational efficiency, the scheme keeps computational efficiency of the scheme for a smoothly and weakly heterogeneous medium (medium without material interfaces).

The second property allows for an arbitrary shape and position of an interface in a uniform spatial grid. The third property means that the number of operations for updating stress, fluid pressure, solid particle velocities and relative fluid particle velocities is the same as in the case of a smoothly and weakly heterogeneous medium; the only difference is that it is necessary to evaluate averaged grid material parameters once before the FD simulation itself.

The developed methodology builds up on methodologies by Moczo *et al.* (2002, 2014, 2019), Kristek & Moczo (2003), Kristek *et al.* (2017, 2019) and proves capabilities of the FD modelling of seismic wave propagation in strongly heterogeneous media.

1.4 Structure of this paper

In this paper, we address the following topics:

(i) transforming equations for the poroelastic medium to equations for the elastic medium,
(ii) averaging of the poroelastic and elastic media,
(iii) updating seismic wavefield using one FD scheme for the poroelastic medium,
(iv) numerical verification of the FD scheme against independent analytical (A), semi-analytical (SA) and SE methods to prove efficiency and accuracy of our FD modelling.

2 EQUATIONS FOR A HETEROGENEOUS POROELASTIC MEDIUM

2.1 Equations for a smoothly heterogeneous medium

Consider a smoothly heterogeneous isotropic poroelastic medium with resistive friction that may be zero, non-zero constant (frequency independent, Biot's model) or frequency dependent (JKD model—after Johnson, Koplik & Dashen 1987). These three types of resistive friction were presented in detail in our previous papers by Moczo *et al.* (2019) and Gregor *et al.* (2021).

The constitutive relations and equations of motion for the 2-D *P-SV* problem in the velocity–stress–pressure formulation may be written as (Moczo *et al.* 2019; Gregor *et al.* 2021)

$$\frac{\partial}{\partial t}\begin{bmatrix}\sigma_{xx}\\ \sigma_{zz}\\ \sigma_{xz}\\ -p\end{bmatrix} = \mathbf{S}_S\ \frac{\partial}{\partial t}\begin{bmatrix}\varepsilon_{xx}\\ \varepsilon_{zz}\\ \varepsilon_{xz}\\ \varepsilon_{w}\end{bmatrix} \tag{1}$$

and

$$\frac{\partial}{\partial t}\begin{bmatrix}v_x\\ -q_x\\ v_z\\ -q_z\end{bmatrix} = \mathbf{R}_S\begin{bmatrix}\dfrac{\partial \sigma_{xx}}{\partial x}+\dfrac{\partial \sigma_{xz}}{\partial z}\\ \dfrac{\partial p}{\partial x}\\ P_x\\ \dfrac{\partial \sigma_{zz}}{\partial z}+\dfrac{\partial \sigma_{xz}}{\partial x}\\ \dfrac{\partial p}{\partial z}\\ P_z\end{bmatrix} \tag{2}$$

The matrices $\mathbf{S}_S$ and $\mathbf{R}_S$ have the following forms:

$$\mathbf{S}_S \equiv \left[\begin{array}{cccc}\Lambda+\alpha^2 M & \lambda_m+\alpha^2 M & 0 & \alpha M\\ \lambda_m+\alpha^2 M & \Lambda+\alpha^2 M & 0 & \alpha M\\ 0 & 0 & 2\mu & 0\\ \alpha M & \alpha M & 0 & \mathrm{M}\end{array}\right] \tag{3}$$

$$\mathbf{R}_S \equiv \frac{1}{m\rho-\rho_f^2}\left[\begin{array}{cccccc}m & \rho_f & \rho_f B & 0 & 0 & 0\\ \rho_f & \rho & \rho B & 0 & 0 & 0\\ 0 & 0 & 0 & m & \rho_f & \rho_f B\\ 0 & 0 & 0 & \rho_f & \rho & \rho B\end{array}\right] \tag{4}$$

In case of the JKD frequency-dependent resistive friction, there are additional equations for diffusive memory variables ψ_n^i ; $i \in \{x,\ z\}$, $n = 1, ..., N$, appearing in the formal wavefield variables P_x and P_z. Denoting

$$\boldsymbol{\psi}^i \equiv \left[\psi_1^i,\ \psi_2^i, ..., \psi_{N-1}^i,\ \psi_N^i\right]^{\mathrm{T}} \tag{5}$$

the additional equations for the diffusive memory variables may be written as

$$\frac{\partial}{\partial t}\,\boldsymbol{\psi}^i = -\left(\mathbf{D}_S+\boldsymbol{\Omega}_S\right)\begin{bmatrix}\dfrac{\partial \sigma_{ij}}{\partial x_j}\\ \dfrac{\partial p}{\partial x_i}\\ P_i\\ q_i\\ \boldsymbol{\psi}^i\end{bmatrix} \tag{6}$$

The matrices $\mathbf{D}_S$ and $\boldsymbol{\Omega}_S$ have the following forms:

$$\mathbf{D}_S \equiv \begin{bmatrix}\rho_f & \rho & \rho B & 0 & 0 & 0 & \cdots & 0 & 0\\ \rho_f & \rho & \rho B & 0 & 0 & 0 & 0 & \cdots & 0\\ \vdots & \vdots & \vdots & \vdots & \vdots & \vdots & \ddots & \vdots & \vdots\\ \rho_f & \rho & \rho B & 0 & 0 & \cdots & 0 & 0 & 0\\ \rho_f & \rho & \rho B & 0 & 0 & 0 & \cdots & 0 & 0\end{bmatrix} \tag{7}$$

Symbol	Name	Units	Relation
u_i	solid displacement component	m	
U_i	fluid displacement component	m	
w_i	displacement component of the fluid relative to the solid matrix		$\phi(U_i - u_i)$
v_i	particle-velocity component of the solid	m/s	$\frac{\partial u_i}{\partial t}$
q_i	particle-velocity component of the fluid relative to the solid matrix	m/s	$\frac{\partial w_i}{\partial t}$
ε_{ij}	solid-matrix strain		$\frac{1}{2}\left(\frac{\partial v_i}{\partial x_j} + \frac{\partial v_j}{\partial x_i}\right)$
ε_w	negative of variation of fluid content		$\frac{\partial w_k}{\partial x_k}$
σ_{ij}	total stress	Pa	
p	pore pressure	Pa	
ψ_n^i	diffusive memory variables	m/s	
P_i	formal wavefield variable in Biot's model	m/s	q_i
	formal wavefield variable in JKD model	$m/s^{1/2}$	$\sum_{l=1}^{N} a_l \psi_l^i(t)$
$i, j \in \{x, z\}$, $n = 1, \ldots, N$			

Figure 2. Wavefield variables of the poroelastic medium.

and

$$\mathbf{\Omega}_S \equiv \begin{bmatrix} 0 & 0 & 0 & -\Omega & \theta_1+\Omega & 0 & \cdots & 0 & 0 \\ 0 & 0 & 0 & -\Omega & 0 & \theta_2+\Omega & 0 & \cdots & 0 \\ \vdots & \vdots & \vdots & \vdots & \vdots & \vdots & \ddots & \vdots & \vdots \\ 0 & 0 & 0 & -\Omega & 0 & \cdots & 0 & \theta_{N-1}+\Omega & 0 \\ 0 & 0 & 0 & -\Omega & 0 & 0 & \cdots & 0 & \theta_N+\Omega \end{bmatrix} \tag{8}$$

The wavefield variables and material parameters, together with basic relations, are listed in Figs 2 and 3, respectively.

2.2 Boundary conditions at a material interface

Consider an interface between two poroelastic materials indicated by the $^+$ and $^-$superscripts, respectively. The boundary conditions at the interface may be written as

$$\begin{aligned} \sigma_{ij}^+ n_j &= \sigma_{ij}^- n_j \\ p^+ &= p^- \\ u_i^+ &= u_i^- \\ w_i^+ n_i &= w_i^- n_i \end{aligned} \tag{9}$$

where n_i is the unit normal to the interface. The Einstein's summation convention for repeating indices is assumed.

Symbol	Name	Units	Relation
solid phase			
ρ_s	density	kg/m^3	
K_s	bulk modulus	Pa	
μ_s	shear modulus	Pa	
fluid phase			
ρ_f	density	kg/m^3	
K_f	bulk modulus	Pa	
η	dynamic viscosity	$Pa\,s$	
solid matrix (drained)			
K_m	bulk modulus	Pa	
μ	shear modulus	Pa	
λ	Lamé elastic coefficient	Pa	$K_m - \mu$
ϕ	porosity		
T	tortuosity		
κ_0	intrinsic permeability	m^2	
saturated porous medium (undrained)			
ρ	total density	kg/m^3	$(1-\phi)\,\rho_s + \phi\,\rho_f$
K_u	bulk modulus	Pa	$K_m + \alpha^2 M$
λ_c	Lamé coefficient	Pa	$K_u - \mu$
Λ		Pa	$\lambda + 2\mu$
α	coefficient of effective stress		$1 - K_m/K_s$
M	coupling modulus between solid and fluid	Pa	$K_s/\left(1-\phi-K_m/K_s+\phi K_s/K_f\right)$
m	mass coupling coefficient	kg/m^3	$T\rho_f/\phi$
b	resistive damping (friction)	$Pa\,s/m^2$	η/κ_0
f_c	Biot characteristic frequency	Hz	$\phi b/\left(T\,\rho_f\right) = \phi\eta/\left(T\,\rho_f\,\kappa_0\right)$
B	formal parameter in Biot's model	$Pa\,s/m^2$	b
	formal parameter in JKD model	$Pa\,s^{1/2}/m^2$	$b/\sqrt{\Omega}$
JKD model			
F	electrical formation factor		$T/\phi = m/\rho_f$
Λ_P	weighted pore-volume to grain-surface ratio	m	
n_J	dimensionless parameter		$n_J = \Lambda_P^2/\left(F\,\kappa_0\right)$
Ω	auxiliary material parameter	Hz	$n_J\,\pi\,f_c/2$
coefficients for diffusive approximation			
a_l	weights	$s^{1/2}$	
θ_l	abscissae	Hz	

Figure 3. Material parameters of the poroelastic medium.

2.3 Equations for the averaging representation of the strongly heterogeneous medium

Moczo *et al.* (2019) and Gregor *et al.* (2021) developed the discrete representation (averaging) of a strongly heterogeneous poroelastic medium (with zero or non-zero constant or frequency-dependent resistive friction) that can include material interfaces. The averaging is based on approximation of the boundary conditions (9) at the material interface. In case of a planar interface (parallel to a Cartesian coordinate plane) between two homogeneous media, the averaging of the material parameters is exact. Otherwise, the averaging is approximate.

The crucial aspect of the discrete material representation is that the numbers of non-zero elements in matrices for the averaged medium are the same as those in the matrices for the smoothly heterogeneous medium. This means that the number of algebraic operations for updating wavefield variables is the same as in the smoothly heterogeneous medium.

The other important aspect is that the averaging was developed for the velocity–stress–pressure staggered-grid scheme with the second-order accuracy in time and fourth-order accuracy in space.

The corresponding FD scheme has a subcell resolution capability.

The equations for the averaged poroelastic medium are summarized in Appendix A.

3 TRANSFORMING EQUATIONS FOR THE POROELASTIC MEDIUM TO EQUATIONS FOR THE ELASTIC MEDIUM

First, we will briefly summarize how to 'transform' the smooth poroelastic medium into the strictly elastic medium using limit values of the poroelastic material parameters. Then, we will develop the corresponding 'transformation' for the averaged poroelastic medium because we will need such 'transformation' for developing relations for the averaged medium consisting of the poroelastic and elastic parts.

3.1 Smoothly heterogeneous medium

Bourbié *et al.* (1987) presented limit values of the poroelastic material parameters for which the (two-component) poroelastic medium becomes a strictly (single-component) elastic medium. As it will be obvious from the following considerations, Bourbié *et al.* (1987) reasonably considered the constitutive relations in the form in which the pore pressure is explicitly present in the relations for the stress components. Also, they considered equations of motion in which both particle velocities are explicitly present. Correspondingly, the constitutive relations and equations of motion may be written as

$$\frac{\partial \sigma_{ij}}{\partial t} = \lambda_m \frac{\partial \varepsilon_{kk}}{\partial t} \delta_{ij} + 2\mu \frac{\partial \varepsilon_{ij}}{\partial t} - \alpha \frac{\partial p}{\partial t} \delta_{ij}$$

$$\frac{\partial p}{\partial t} = -\alpha M \frac{\partial \varepsilon_{kk}}{\partial t} - M \frac{\partial \varepsilon_w}{\partial t} \tag{10}$$

$$\rho \frac{\partial v_i}{\partial t} = \frac{\partial \sigma_{ij}}{\partial x_j} - \rho_f \frac{\partial q_i}{\partial t}$$

$$\rho_f \frac{\partial q_i}{\partial t} = -\frac{1}{m} \left(\rho_f \frac{\partial p}{\partial x_i} + \rho_f^2 \frac{\partial v_i}{\partial t} + \rho_f B P_i \right) \tag{11}$$

Consider zero coefficient of the effective stress α and zero porosity ϕ:

$$\alpha = \phi = 0 \tag{12}$$

Then

(i) Relation $\alpha = 0$ implies equality of the bulk moduli of the solid, drained solid matrix and undrained poroelastic medium:

$$K_s = K_m = K_u \tag{13}$$

(ii) Relations $K_s = K_m$ and $\phi = 0$ together imply an infinite value of the coupling modulus between solid and fluid:

$$M \to \infty \tag{14}$$

(iii) As porosity $\phi \to 0$, the total fluid volume becomes too small and loses capability to flow through the medium. The loss of capability of the fluid to flow can be also due to tortuosity $T \to \infty$. Thus, in addition to $\phi \to 0$ we may also consider

$$T \to \infty \tag{15}$$

[We may note the relation between ϕ and T found by Berryman (1980) for the solid matrix: $T = 1 + r(1/\phi - 1)$, where, e.g. $r = 1/2$ for spherical grains.]

Guan & Hu (2011) noted equality of the total, solid and fluid densities,

$$\rho = \rho_s = \rho_f \tag{16}$$

and equality of the bulk moduli of the solid, drained solid matrix, undrained poroelastic medium medium and fluid

$$K_s = K_m = K_u = K_f \tag{17}$$

In order to 'transform' the poroelastic medium into the strictly elastic medium, it is necessary (and enough) to apply the first equality in eq. (16) in addition to relations (12)–(15). In the following, we apply relations (12)–(16) to eqs (10) and (11).

Due to the zero coefficient of the effective stress, $\alpha = 0$, the pore pressure p is eliminated from the constitutive equations for the stress components. This is consistent with the fact that there is no need to calculate the pore pressure p in the elastic medium. Thus, eq. (10) reduce to

$$\frac{\partial \sigma_{ij}}{\partial t} = \lambda_m \frac{\partial \varepsilon_{kk}}{\partial t} \delta_{ij} + 2\mu \frac{\partial \varepsilon_{ij}}{\partial t} \tag{18}$$

Due to the zero porosity, $\phi = 0$, the inverse value of the mass coupling coefficient m becomes zero:

$$\left.\frac{1}{m}\right|_{\phi=0} = \left.\frac{\phi}{T\rho_f}\right|_{\phi=0} = 0 \tag{19}$$

Considering relations (19) and assuming that the formal parameter B does not reach an infinite value, the right-hand side of the second of eq. (11) vanishes:

$$\rho_f \frac{\partial q_i}{\partial t} = 0 \tag{20}$$

Recall that parameter B serves to account for the resistive friction in the Biot's or JKD models. The parameter has no meaning for the elastic medium but given the infinite value of the mass coupling coefficient m, it is enough to formally assume that its value is limited.

If we assume zero initial condition for the fluid particle velocity q_i in eq. (20), equations of motion (11) reduce to

$$\rho \frac{\partial v_i}{\partial t} = \frac{\partial \sigma_{ij}}{\partial x_j} \tag{21}$$

We conclude that setting the zero coefficient of the effective stress, $\alpha = 0$, in eqs (10) and the zero inverse value of the mass coupling coefficient, $1/m = 0$, in eq. (11) leads to eqs (18) and (21), that is equations for the elastic medium.

Because we are 'transforming ' the poroelastic medium which is also described by the diffusive memory variables, we have to look also at the system of equations for the diffusive memory variables (6). If we apply relation (19) for the mass coupling coefficient m to the system of equations (6) and consider $\Omega = 0$ due to $\phi = 0$, the system reduces to

$$\frac{\partial \psi_n^i}{\partial t} = -\theta_n \psi_n^i; \quad i \in \{x, z\}, n = 1, \ldots, N \tag{22}$$

It follows from eq. (22) and the initial boundary conditions that the diffusive memory variables are equal to zero all the time. Consequently, the system of equations for the diffusive memory variables can be disregarded.

Eventually, we have to 'transform' also the boundary conditions (9). They easily reduce to the boundary conditions at a material interface between two elastic materials:

$$\begin{aligned} \sigma_{ij}^+ n_j &= \sigma_{ij}^- n_j \\ u_i^+ &= u_i^- \end{aligned} \tag{23}$$

The meaning of the superscripts and n_j is the same as in relations (9).

3.2 Averaged medium

The constitutive relations for the averaged poroelastic medium for 2-D *P-SV* problem, eqs (A1) and (A3), may be written, consistently with the constitutive relations in system (10), as

$$\frac{\partial}{\partial t}\begin{bmatrix} \sigma_{xx} \\ \sigma_{zz} \\ \sigma_{xz} \\ -p \end{bmatrix} = \begin{bmatrix} XX & XZ & 0 & 0 & XP \\ XZ & ZZ & 0 & 0 & ZP \\ 0 & 0 & 2\langle\mu\rangle^{Hxz} & 0 & 0 \\ \frac{XP}{\Psi} & \frac{ZP}{\Psi} & 0 & \frac{1}{\Psi} & 0 \end{bmatrix} \frac{\partial}{\partial t}\begin{bmatrix} \varepsilon_{xx} \\ \varepsilon_{zz} \\ \varepsilon_{xz} \\ \varepsilon_w \\ -p \end{bmatrix} \tag{24}$$

The main point with this form of the constitutive relation is that the averaged parameter Ψ appears just in the relation for the fluid pore pressure which is not defined in the elastic medium and thus not evaluated. The averaged material parameters XX, ZZ and XZ, formally unchanged, are evaluated for λ^E and Λ^E representing the elastic medium. Parameters XP and ZP are equal to zero for the zero coefficient of effective stress, $\alpha = 0$. Thus, they eliminate the pore pressure p from relations for the stress components. Since there is no need to calculate the pore pressure p in the elastic medium, the relation for the pore pressure p may be disregarded. Consequently, the constitutive relations

(24) for the averaged poroelastic medium reduce to

$$\frac{\partial}{\partial t}\begin{bmatrix}\sigma_{xx}\\ \sigma_{zz}\\ \sigma_{xz}\end{bmatrix}=\begin{bmatrix}XX & XZ & 0\\ XZ & ZZ & 0\\ 0 & 0 & 2\langle\mu\rangle^{Hxz}\end{bmatrix}\frac{\partial}{\partial t}\begin{bmatrix}\varepsilon_{xx}\\ \varepsilon_{zz}\\ \varepsilon_{xz}\end{bmatrix} \tag{25}$$

that is, to the constitutive relations for the averaged elastic medium (Moczo *et al.* 2014; Kristek *et al.* 2017).

Consider now the equations of motion (A2) for the averaged medium. Relation (16) implies for the auxiliary averaged material parameters F^{ξ}, R^{ξ} and P^{ξ} appearing in matrices $\mathbf{R}_A$ and $\mathbf{D}_A$ (see their definitions in Appendix A), the following equalities: $F^{\xi}\neq 0$, $R^{\xi}\neq 0$ and $P^{\xi}=1$. Relation (19) implies for the auxiliary averaged material parameters G^{ξ}, H^{ξ} and Q^{ξ} appearing in matrices $\mathbf{R}_A$ and $\mathbf{D}_A$ the following equalities: $G^{\xi}=0$, $H^{\xi}=0$ and $Q^{\xi}=0$. Recall again that we assume that the formal parameter B does not reach an infinite value in the elastic medium. Eventually, the auxiliary averaged material parameter S^{ξ} appearing in matrix $\mathbf{R}_A$ attains value $S^{\xi}=1$. Consequently, matrix $\mathbf{R}_A$ in equations of motion (A2) reduces to

$$\mathbf{R}_A=\left[\begin{array}{cccccc}\frac{\langle F^x\rangle^z}{\langle S^x\rangle^z} & 0 & 0 & 0 & 0 & 0\\ 0 & 0 & 0 & 0 & 0 & 0\\ 0 & 0 & 0 & \frac{\langle F^z\rangle^x}{\langle S^z\rangle^x} & 0 & 0\\ 0 & 0 & 0 & 0 & 0 & 0\end{array}\right] \tag{26}$$

where

$$\frac{\langle F^x\rangle^z}{\langle S^x\rangle^z}=\frac{1}{\langle\langle\rho_s\rangle^x\rangle^z},\quad \frac{\langle F^z\rangle^x}{\langle S^z\rangle^x}=\frac{1}{\langle\langle\rho_s\rangle^z\rangle^x} \tag{27}$$

Due to eq. (26), the equations of motion (A2) are reduced to the equations for the averaged elastic medium (Moczo *et al.* 2014; Kristek *et al.* 2017):

$$\begin{bmatrix}\frac{\partial v_x}{\partial t}\\ \frac{\partial v_z}{\partial t}\end{bmatrix}=\begin{bmatrix}\frac{1}{\langle\langle\rho_s\rangle^x\rangle^z} & 0\\ 0 & \frac{1}{\langle\langle\rho_s\rangle^z\rangle^x}\end{bmatrix}\begin{bmatrix}\frac{\partial\sigma_{xx}}{\partial x}+\frac{\partial\sigma_{xz}}{\partial z}\\ \frac{\partial\sigma_{zz}}{\partial z}+\frac{\partial\sigma_{xz}}{\partial x}\end{bmatrix} \tag{28}$$

Consider now the system of equations for the diffusive memory variables (6) for the averaged poroelastic medium. Using relation (19) for the mass coupling coefficient m in the system, the system reduces to

$$\frac{\partial\psi_n^i}{\partial t}=-\theta_n\,\psi_n^i;\quad i\in\{x,z\},n=1,\ldots,N \tag{29}$$

where $\Omega=0$ due to $\phi=0$. Due to the zero initial conditions the diffusive memory variables are equal to zero all the time. Consequently, the system of equations for the diffusive memory variables can be disregarded which is correct for the strictly elastic medium.

Let us note that the obtained systems of eqs (25) and (28) correspond to the orthorhombic averaging (Moczo *et al.* 2014; Kristek *et al.* 2017) for the strongly heterogeneous medium with material interfaces. The orthorhombic averaging of the strongly heterogeneous elastic medium is based on approximation of the boundary conditions (23) at the material interface. In case of a planar interface (parallel to a Cartesian coordinate plane) between two homogeneous media, the averaging of the material parameters is exact.

4 THE UNIFYING EQUATION FOR THE AVERAGED POROELASTIC MEDIUM

Gregor *et al.* (2021) presented the unifying matrix-form equation for the averaged poroelastic medium. The unifying form is suitable concise form for the so-called partitioning into the non-stiff and stiff systems.

Recall that in the case of the poroelastic medium with non-zero constant resistive friction (Biot's model) or frequency-dependent resistive friction, the equations of motion include the so-called viscous dissipation terms. In the equations for the solid particle-velocity components v_x and v_z they are $(\langle H^x\rangle^z/\langle S^x\rangle^z)P_x$ and $(\langle H^z\rangle^x/\langle S^z\rangle^x)P_z$, respectively. In the equations for the fluid particle-velocity components q_x and q_z they are $(\langle P^x\rangle^z\langle H^x\rangle^z/\langle S^x\rangle^z)\,P_x$ and $(\langle P^z\rangle^x\langle H^z\rangle^x/\langle S^z\rangle^x)\,P_z$.

The presence of the dissipation terms in the equations of motion implies that the equations behave as a stiff system in the so-called low-frequency regime (the frequency range of the computed wavefield is well below the Biot's characteristic frequency). According to Iserles (2009), a differential equation is stiff if its numerical solution by some method requires a significant reduction of the step size to avoid instability. A very small time step is due to a relatively very small wavelength of the diffusive slow P wave and large velocity of the fast P wave. The problem can be circumvented by using the partition method suggested by Carcione & Quiroga-Goode (1995).

Due to the difference in the forms of the incorporated constitutive relations for the averaged poroelastic medium, explained above, here we need a unifying equation different from that presented by Gregor *et al.* (2021).

4.1 Unifying equation

We can incorporate constitutive relations (24), eqs (A8)–(A11), equations of motion (A2), eqs (A4) and (A12), additional equations for diffusive memory variables (A5), and eqs (A6), (A7) and (A13) for the averaged poroelastic medium in the unifying matrix-form equation

$$T_{pq}\frac{\partial\,\vec{Q}_p}{\partial\,t}+X_{pq}\frac{\partial\,\vec{Q}_p}{\partial\,x}+Z_{pq}\frac{\partial\,\vec{Q}_p}{\partial\,z}=-S_{pq}\,\vec{Q}_p \tag{30}$$

where vector $\vec{Q}_p$

$$\vec{Q}_p\equiv\left(v_x,q_x,\psi_1^x,\ldots,\psi_N^x,v_z,q_z,\psi_1^z,\ldots,\psi_N^z,\sigma_{xx},\sigma_{xz},\sigma_{zz},p\right)^T \tag{31}$$

has $p=2\,N+8$ elements ($N=3$ being sufficient, Blanc 2013). Relatively cumbersome matrices T_{pq}, X_{pq}, Z_{pq} and S_{pq} are shown in Appendix B.

As mentioned above, the unified equation (30) is different from the analogous equation (57) in Gregor *et al.* (2021). They used relation (A1) with matrix (A3). Here, we incorporated relation in form (24). The difference is in the presence of the pore pressure on the right-hand side of eq. (24) and corresponding modification of the matrix. The pore pressure is not explicitly present in relation (A1) and matrix (A3) has only four columns. Note that both forms are fully equivalent for the averaged poroelastic medium. The reason for using form (24) in this paper is the intended incorporation of the poroelastic and strictly elastic parts of the medium. This will be well seen later.

Here, we present partitioning applied to our system (30).

4.2 Partitioning of the unifying equation into the stiff and non-stiff systems

Moczo *et al.* (2019) applied the partitioning in the FD modelling of seismic waves in the averaged poroelastic medium with constant resistive friction. Gregor *et al.* (2021) applied the partitioning to the unifying equation for the averaged poroelastic medium with a constant resistive friction or with the JKD frequency-dependent resistive friction and its diffusive approximation. Here, we apply the partitioning to the unified equation (30).

Term $S_{pq}\,\vec{Q}_p$ in eq. (30) includes the viscous dissipation term. Recall that the presence of the dissipation term implies that eq. (30) behaves as a stiff system in the so-called low-frequency regime. System (30) may be partitioned into the non-stiff and stiff systems, respectively:

$$T_{pq}\frac{\partial\,\vec{Q}_p}{\partial\,t}+X_{pq}\frac{\partial\,\vec{Q}_p}{\partial\,x}+Z_{pq}\frac{\partial\,\vec{Q}_p}{\partial\,z}=0 \tag{32}$$

and

$$T_{pq}\frac{\partial\,\vec{Q}_p}{\partial\,t}=-S_{pq}\,\vec{Q}_p \tag{33}$$

The point is that the stiff system can be solved analytically and, consequently, does not require a numerical integration. The analytical solution of the stiff system is then used in the non-stiff system. Denoting

$${}^i\vec{Q}\equiv\left(v_i,q_i,\boldsymbol{\psi}^i\right)^T;\quad i\in\{x,z\} \tag{34}$$

and using definition (B11, Appendix B), the stiff system (33) may be written as

$$T_{pq}\frac{\partial}{\partial t}\begin{pmatrix}{}^x\vec{Q}\\ {}^z\vec{Q}\\ \sigma_{xx}\\ \sigma_{xz}\\ \sigma_{zz}\\ p\end{pmatrix}=\begin{pmatrix}S^x_{N+2,\,N+2} & 0_{N+2,\,N+2} & 0_{N+2,\,4}\\ 0_{N+2,\,N+2} & S^z_{N+2,\,N+2} & 0_{N+2,\,4}\\ 0_{4,\,N+2} & 0_{4,\,N+2} & 0_{4,\,4}\end{pmatrix}\begin{pmatrix}{}^x\vec{Q}\\ {}^z\vec{Q}\\ \sigma_{xx}\\ \sigma_{xz}\\ \sigma_{zz}\\ p\end{pmatrix} \tag{35}$$

Because $S^x_{N+2,\,N+2}$ and $S^z_{N+2,\,N+2}$ do not depend on time, system (35) can be solved analytically for ${}^x\vec{Q}$ and ${}^z\vec{Q}$:

$${}^i\vec{Q}^*\Big|^{m+1/2}\equiv\begin{pmatrix}v_i^*\big|^{m+1/2}\\ q_i^*\big|^{m+1/2}\\ \boldsymbol{\psi}^{i*}\big|^{m+1/2}\end{pmatrix}=\exp\left(-S^i_{N+2,N+2}\,\Delta\right)\;{}^i\vec{Q}\Big|^{m-1/2};\quad i\in\{x,z\} \tag{36}$$

Here, '$*$' indicates an analytical solution of (35) and the vertical bar '|' is used to indicate the time level. The matrix exponentials $\exp\left(-\,S^i_{N+2,N+2}\Delta\right)$; $i\in\{x,z\}$, can be computed by, for example, the 'ExpoRkit' Fortran package (Hansen 2018) based on the scaling and

squaring algorithm with the Padé approximation. The resulting matrix for $\exp(-S^i_{N+2,N+2}\Delta)$ is

$$\exp\left(-S^i_{N+2,\,N+2}\,\Delta\right) \approx \tilde{S}^i_{N+2,\,N+2} = \begin{pmatrix} \tilde{s}^{v_i}_{v_i} & \tilde{s}^{q_i}_{v_i} & \tilde{s}^{\psi^i_1}_{v_i} & \cdots & \tilde{s}^{\psi^i_N}_{v_i} \\ \tilde{s}^{v_i}_{q_i} & \tilde{s}^{q_i}_{q_i} & \tilde{s}^{\psi^x_1}_{q_i} & \cdots & \tilde{s}^{\psi^x_N}_{q_i} \\ \tilde{s}^{v_i}_{\psi^i_1} & \tilde{s}^{q_i}_{\psi^i_1} & \tilde{s}^{\psi^i_1}_{\psi^i_1} & \cdots & \tilde{s}^{\psi^i_N}_{\psi^i_1} \\ \vdots & \vdots & \vdots & \cdots & \vdots \\ \tilde{s}^{v_i}_{\psi^i_N} & \tilde{s}^{q_i}_{\psi^i_N} & \tilde{s}^{\psi^i_1}_{\psi^i_N} & \cdots & \tilde{s}^{\psi^i_N}_{\psi^i_N} \end{pmatrix}; \quad i \in \{x, z\} \tag{37}$$

Using ${}^x\vec{Q}$ and ${}^z\vec{Q}$ in eqs (36), and $\tilde{S}^x$ and $\tilde{S}^z$ in eq. (37), we obtain

$${}^i\vec{Q}^*\Big|^{m+1/2} = \tilde{S}^i_{N+2,N+2}\;{}^i\vec{Q}\Big|^{m-1/2}; \quad i \in \{x, z\} \tag{38}$$

Variables ${}^i\vec{Q}^*|^{m+1/2}; i \in \{x, z\}$ enter the non-stiff explicit scheme for eq. (32).

Whereas simplification of matrices X_{pq}, Z_{pq} and T_{pq} in case of transforming poroelastic medium into elastic medium is obvious—based on Section 3.2, simplification of matrix $\tilde{S}^i_{N+2,N+2}$ requires explanation. The explanation is given in Appendix C.

5 AVERAGING OF THE POROELASTIC AND ELASTIC MEDIA

We want our model of the medium to consist of poroelastic and (strictly) elastic parts. At the same time, we want to use only one FD scheme for simulating wavefield in the entire model. Therefore, we need to develop an averaging representation of the strongly heterogeneous medium consisting of the poroelastic and elastic parts. A discrete representation of the averaged medium must properly represent poroelastic and elastic behaviours of the corresponding original poroelastic and elastic parts, respectively, as well as their interaction.

5.1 Material parameters

The poroelastic and elastic parts will be indicated by superscripts P and E, respectively. An interface between the P and E media will be called a P/E interface. We assume that the P/E interface may have an arbitrary geometric shape and position in a uniform FD grid.

Obviously, we have to determine averaged material parameters in matrices T_{pq}, X_{pq}, Z_{pq} and S_{pq} appearing in the matrix-form equation (30). Let h be a grid spacing of a uniform rectangular grid. Consider an $h \times h$ area centred at a grid position of a wavefield variable, that is, the area of averaging. We need to consider three possible situations with respect to the wavefield variable:

(i) fully poroelastic—the entire averaging area is inside the P medium,
(ii) fully elastic—the entire averaging area is inside the E medium,
(iii) mixed—the averaging area is crossed by one or more P/E interfaces.

Material parameters of the poroelastic medium (λ^P, μ^P, Λ^P, α^P, M^P and ρ^P_f, ρ^P, m^P, B^P) are obviously all non-zero and finite except parameter B^P which is equal to zero in case of the medium with zero resistive friction.

Recall considerations in Section 3.1 on obtaining equations of the elastic medium from the equations for the poroelastic medium by adjusting values of several poroelastic parameters. Parameters λ^E, μ^E, Λ^E, ρ^E are always non-zero. For the elastic medium, we will formally consider the coefficient of effective stress $\alpha^E = 0$, mass coupling coefficient $m^E \to \infty$ and the coupling modulus between solid and fluid $M^E \to \infty$. We assume that the formal parameter B^E does not reach an infinite value.

5.2 Boundary conditions

Recall that our averaging of the poroelastic medium, matrices (A3) and (A4), is based on approximation of the boundary conditions (9) at the interface between two poroelastic media. Also recall that the averaging of the elastic medium, matrices in relations (25) and (28), is based on approximation of the boundary conditions (23) at the interface between two elastic media. To include P/E interfaces, we need averaging based on the corresponding boundary conditions (Lovera 1987):

$$\begin{aligned} \sigma^P_{ij} n_j &= \sigma^E_{ij} n_j \\ -p^P &= \sigma^E_{ij} n_i n_j \\ u^P_i &= u^E_i \\ w^P_i n_i &= 0 \end{aligned} \tag{39}$$

averaging area fully		mixed averaging area
elastic	**poroelastic**	
parameters at the grid position of σ_{xx}, σ_{zz} and p		
$XX\left(\lambda^E, \Lambda^E\right) \neq 0$	$XX\left(\lambda^P, \Lambda^P\right) \neq 0$	$XX\left(\lambda^E, \Lambda^E, \lambda^P, \Lambda^P\right) \neq 0$
$ZZ\left(\lambda^E, \Lambda^E\right) \neq 0$	$ZZ\left(\lambda^P, \Lambda^P\right) \neq 0$	$ZZ\left(\lambda^E, \Lambda^E, \lambda^P, \Lambda^P\right) \neq 0$
$XZ\left(\lambda^E, \Lambda^E\right) \neq 0$	$XZ\left(\lambda^P, \Lambda^P\right) \neq 0$	$XZ\left(\lambda^E, \Lambda^E, \lambda^P, \Lambda^P\right) \neq 0$
$XP\left(\lambda^E, \Lambda^E, \alpha^E\right) = 0$	$XP\left(\lambda^P, \Lambda^P, \alpha^P\right) \neq 0$	$XP\left(\lambda^E, \Lambda^E, \alpha^E, \lambda^P, \Lambda^P, \alpha^P\right) \neq 0$
$ZP\left(\lambda^E, \Lambda^E, \alpha^E\right) = 0$	$ZP\left(\lambda^P, \Lambda^P, \alpha^P\right) \neq 0$	$ZP\left(\lambda^E, \Lambda^E, \alpha^E, \lambda^P, \Lambda^P, \alpha^P\right) \neq 0$
$\Psi\left(\Lambda^E, \alpha^E, M^E\right) = 0$	$\Psi\left(\Lambda^P, \alpha^P, M^P\right) \neq 0$	$\Psi\left(\Lambda^E, \alpha^E, M^E, \Lambda^P, \alpha^P, M^P\right) \neq 0$
$XP/\Psi := 0$	$XP/\Psi \neq 0$	$XP/\Psi \neq 0$
$ZP/\Psi := 0$	$ZP/\Psi \neq 0$	$ZP/\Psi \neq 0$
$1/\Psi := 0$	$1/\Psi \neq 0$	$1/\Psi \neq 0$
parameter at the grid position of σ_{xz}		
$\left\langle \mu^E \right\rangle^{Hxz} \neq 0$	$\left\langle \mu^P \right\rangle^{Hxz} \neq 0$	$\left\langle \mu\left(\mu^E, \mu^P\right) \right\rangle^{Hxz} \neq 0$
parameters at the grid position of v_x, q_x, ψ_1^x, …, ψ_N^x		
$\left\langle F^x\left(\rho^E\right) \right\rangle^z \neq 0$	$\left\langle F^x\left(\rho_f^P\right) \right\rangle^z \neq 0$	$\left\langle F^x\left(\rho^E, \rho_f^P\right) \right\rangle^z \neq 0$
$\left\langle G^x\left(m^E\right) \right\rangle^z = 0$	$\left\langle G^x\left(m^P\right) \right\rangle^z \neq 0$	$\left\langle G^x\left(m^E, m^P\right) \right\rangle^z = 0$
$\left\langle H^x\left(m^E, B^E\right) \right\rangle^z := 0$	$\left\langle H^x\left(m^P, B^P = 0\right) \right\rangle^z = 0$ $\left\langle H^x\left(m^P, B^P \neq 0\right) \right\rangle^z \neq 0$	$\left\langle H^x\left(m^E, B^E, m^P, B^P\right) \right\rangle^z := 0$
$\left\langle P^x\left(\rho^E\right) \right\rangle^z \neq 0$	$\left\langle P^x\left(\rho_f^P, \rho^P\right) \right\rangle^z \neq 0$	$\left\langle P^x\left(\rho^E, \rho_f^P, \rho^P\right) \right\rangle^z \neq 0$
$\left\langle R^x\left(\rho^E\right) \right\rangle^z \neq 0$	$\left\langle R^x\left(\rho_f^P\right) \right\rangle^z \neq 0$	$\left\langle R^x\left(\rho^E, \rho_f^P\right) \right\rangle^z \neq 0$
$\left\langle Q^x\left(\rho^E, m^E\right) \right\rangle^z = 0$	$\left\langle Q^x\left(\rho_f^P, m^P\right) \right\rangle^z \neq 0$	$\left\langle Q^x\left(\rho^E, m^E, \rho_f^P, m^P\right) \right\rangle^z = 0$
$\left\langle \frac{G^x\left(m^E\right)}{R^x\left(\rho^E\right)} \right\rangle^z = 0$	$\left\langle \frac{G^x\left(m^P\right)}{R^x\left(\rho_f^P\right)} \right\rangle^z \neq 0$	$\left\langle \frac{G^x\left(m^E, m^P\right)}{R^x\left(\rho^E, \rho_f^P\right)} \right\rangle^z = 0$

Figure 4. Summary of the averaged material parameters. Symbol ':=' means assigning the value. Parameters at the grid position of v_z, q_z, ψ_1^z, …, ψ_N^z are determined analogously.

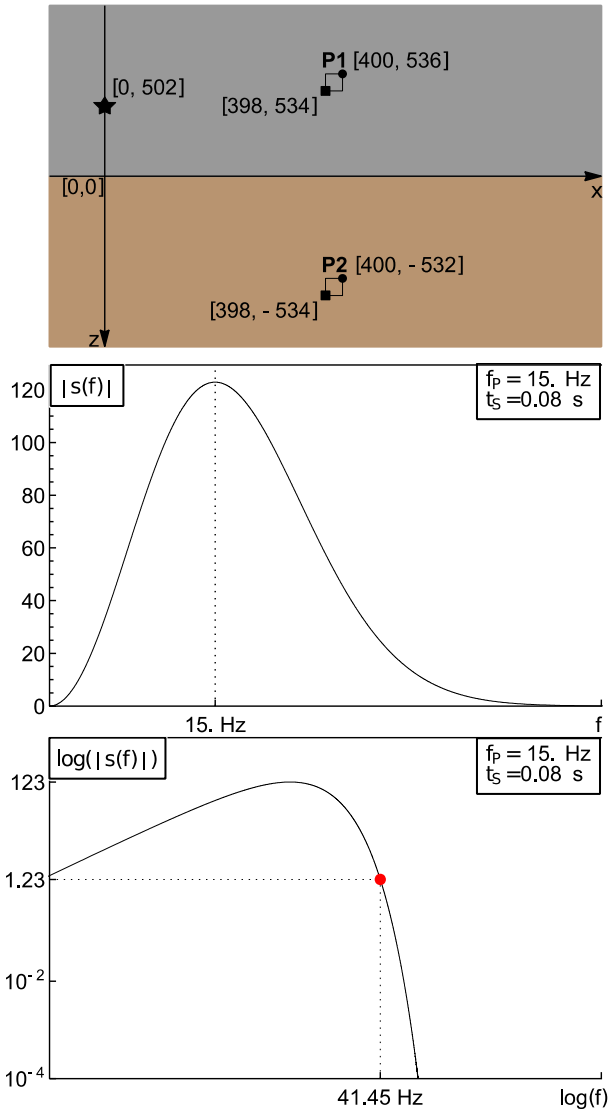

Figure 5. Upper panel: source (star)-receiver (P1 and P2) configuration in the model of two half-spaces. The numbers mean values in m. The upper poroelastic half-space is in a horizontal planar contact with the lower perfectly elastic half-space. Middle panel: amplitude spectrum of the source signal. Bottom panel: log–log spectrum of the source signal. The amplitude falls from its maximum by two orders at frequency of 41.45 Hz.

5.3 Averaging of material parameters in the constitutive relations

The averaging methodology developed by Moczo *et al.* (2019) for the strongly heterogeneous poroelastic medium can be also applied in the case of the strongly heterogeneous medium composed of the poroelastic and elastic parts.

5.3.1 Shear stress-tensor component at a planar interface perpendicular to the x axis

For the two half-spaces (indicated by the ^{P} and ^{E} superscripts) in a contact we may write in general

$$\sigma_{xz} = 2\mu^{E}\,\varepsilon^{E}_{xz}, \quad \sigma_{xz} = 2\mu^{P}\,\varepsilon^{P}_{xz} \tag{40}$$

or

$$\frac{1}{\mu^{E}}\,\sigma_{xz} = 2\,\varepsilon^{E}_{xz}, \quad \frac{1}{\mu^{P}}\,\sigma_{xz} = 2\,\varepsilon^{P}_{xz} \tag{41}$$

Considering continuity of σ_{xz} and an arithmetic average $\langle\varepsilon_{xz}\rangle^{x}$ at the interface,

$$\langle\varepsilon_{xz}\rangle^{x} \equiv \tfrac{1}{2}\left(\varepsilon^{E}_{xz} + \varepsilon^{P}_{xz}\right) \tag{42}$$

the summation of eq. (41) leads to relation

$$\sigma_{xz} = 2\,\langle\mu\rangle^{Hx}\,\langle\varepsilon_{xz}\rangle^{x} \tag{43}$$

Symbol	Units	Value
upper poroelastic halfspace		
solid phase		
ρ_s	kg/m^3	2200
K_s	Pa	$6.9 \cdot 10^9$
fluid phase		
ρ_f	kg/m^3	950
K_f	Pa	$2.0 \cdot 10^9$
η	$Pa\,s$	0
solid matrix (drained)		
K_m	Pa	$6.7 \cdot 10^9$
μ	Pa	$3.0 \cdot 10^9$
λ_m	Pa	$4.7 \cdot 10^9$
ϕ		0.4
T		2
velocities		
$VP_{fast}^{\inf}$	m/s	2693
$VP_{slow}^{\inf}$	m/s	1186
$VS^{\inf}$	m/s	1410
lower elastic halfspace		
ρ	kg/m^3	2650
K	Pa	$6.845 \cdot 10^9$
μ	Pa	$4.652 \cdot 10^9$
VP	m/s	2219
VS	m/s	1325

Figure 6. Material parameters in the upper poroelastic and lower elastic half-spaces shown in Fig. 5.

FD		**SE**	
size	$301 \times 468 = 140\,868$	number of elements	360 000
grid spacing	$4\,m$	number of GLL points	5 764 801
PML zone	100	element size	$8\,m$
time step	$8.1 \cdot 10^{-4}\,s$	time step	$10^{-4}\,s$
time window $1\,s$			

Figure 7. Parameters used for the FD and SE simulations. In the SE simulation, Lagrange polynomials of degree 4 are used, leading to 5 GLL integration points irregularly spaced in both directions x and z, and 25 GLL points in one element. In the SE simulation, a regular grid and Stacey absorbing boundary condition on all sides are used.

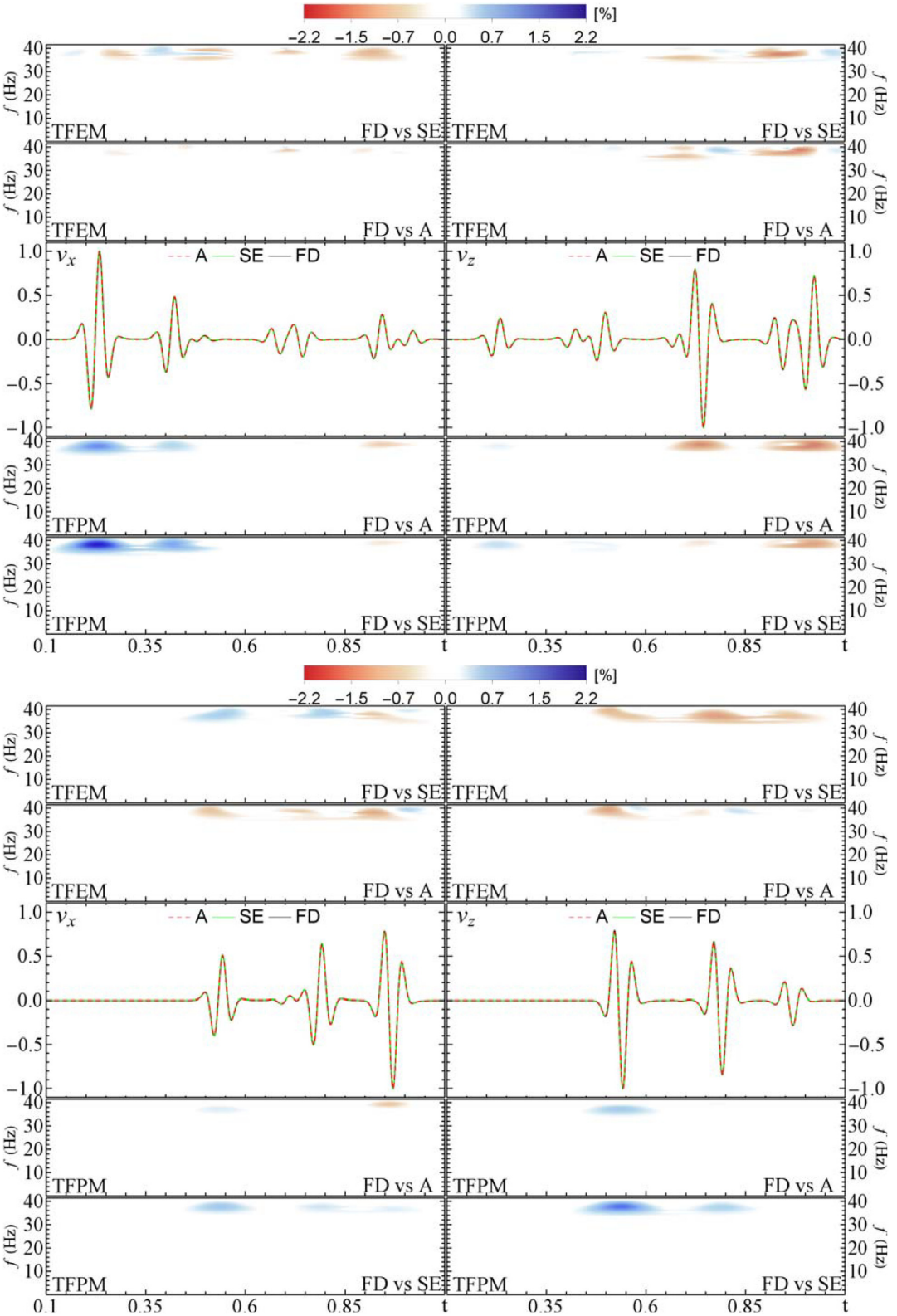

Figure 8. The v_x and v_z seismograms at receivers P1 (upper panel) and P2 (lower panel) in the model of the poroelastic half-space in the planar horizontal contact with the perfectly elastic half-space calculated by the A, SE and FD methods. TFEM and TFPM show the time–frequency representations of the envelope and phase misfits, respectively, between the FD and A seismograms and between the FD and SE seismograms.

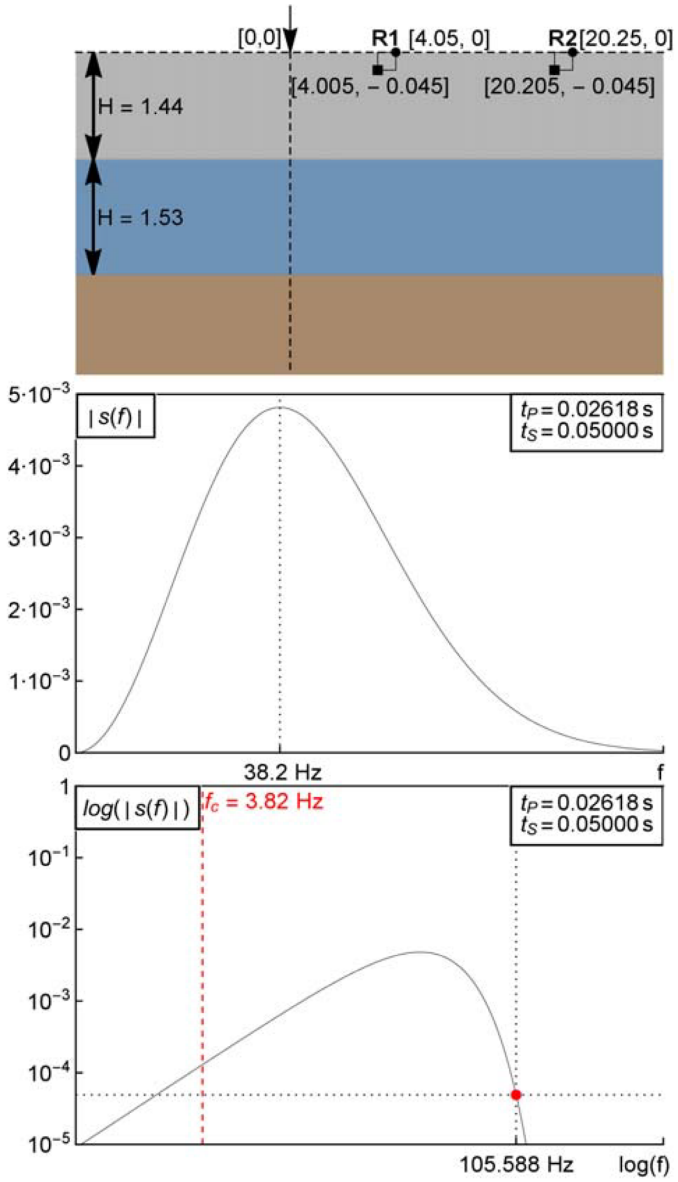

Figure 9. Upper panel: source (vertical arrow)-receiver (R1 and R2) configuration in the model of two layers over a half-space. The numbers mean values in m. Middle panel: amplitude spectrum of the Ricker signal. Bottom panel: log–log spectrum of the Ricker signal. The amplitude falls from its maximum by two orders at frequency of 105.588 Hz.

with the harmonic average of the shear moduli

$$\langle \mu \rangle^{Hx} \equiv \frac{2}{\frac{1}{\mu^E} + \frac{1}{\mu^P}} \tag{44}$$

Thus, continuity of σ_{zx} and the arithmetic averaging of the discontinuous ε_{zx} imply the harmonic averaging of the shear moduli, $\langle \mu \rangle^{Hx}$, in the stress–strain relation at the interface. Relation (43) has the same form as the relation for a point in a smooth medium and is consistent with the interface boundary conditions. Relation (43) is the same as in the case of the interface between two elastic media.

5.3.2 Normal stress-tensor components at a planar interface perpendicular to the x axis

For two half-spaces in contact we may write

$$\begin{aligned} \sigma_{xx} &= \Lambda^E \, \varepsilon^E_{xx} + \lambda^E \varepsilon_{zz} \\ \sigma_{xx} &= \Lambda^P \, \varepsilon^P_{xx} + \lambda^P \varepsilon_{zz} - \alpha^P p^P \end{aligned} \tag{45}$$

Symbol	Units	Upper layer	Lower layer	halfspace
solid phase				
ρ_s	kg/m^3	2650	2650	2650
K_s	Pa	$36\cdot10^9$	$36\cdot10^9$	$36\cdot10^9$
fluid phase				
ρ_f	kg/m^3	1000	1000	1000
K_f	Pa	$2.37\cdot10^9$	$2.37\cdot10^9$	$2.37\cdot10^9$
η	$Pa\,s$	$1\cdot10^{-3}$	$1\cdot10^{-3}$	$1\cdot10^{-3}$
solid matrix (drained)				
K_m	Pa	$2.66068\cdot10^8$	$2.66068\cdot10^9$	$5.32136\cdot10^{10}$
μ	Pa	$1\cdot10^8$	$1\cdot10^9$	$2\cdot10^{10}$
λ_m	Pa	$1.66068\cdot10^8$	$1.66068\cdot10^9$	$3.32136\cdot10^{10}$
ϕ		0.3	0.3	0.3
T		1.25	1.25	1.25
κ_0	m^2	$1\cdot10^{-8}$	$1\cdot10^{-10}$	$1\cdot10^{-11}$
saturated porous medium (undrained)				
λ_c	Pa	$5.9723\cdot10^8$	$3.0277\cdot10^8$	$1.9303\cdot10^{10}$
b	$Pa\,s\,m^{-2}$	$1\cdot10^5$	$1\cdot10^8$	$1\cdot10^8$
f_c	Hz	3.82	381.97	3819.72
n_J		8	8	8
velocities				
$VP_{fast}^{\inf}$	m/s	1945	2143	6399
$VP_{slow}^{\inf}$	m/s	288	833	1461
$VS^{\inf}$	m/s	229	723	3232

Figure 10. Material parameters in the 3P-B and 3P-JKD models of the poroelastic layers over a poroelastic half-space.

Symbol	Units	Lower layer	halfspace
ρ	kg/m^3	2155	2155
K	Pa	$8.6182\cdot10^9$	$55.3918\cdot10^9$
μ	Pa	$1\cdot10^9$	$2\cdot10^{10}$
λ	Pa	$7.6171\cdot10^9$	$35.3918\cdot10^9$
velocities			
VP	m/s	2143	6399
VS	m/s	723	3232

Figure 11. Material parameters in the lower layer and half-space in the P-B-EE and P-JKD-EE models of the poroelastic layer over an elastic layer and half-space. Material parameters of the upper layer are the same as those for the upper layer in Fig. 10

number of grid cells	$960 \times 59 = 56\,640$
grid spacing	$0.09\ m$
PML zone	100
time step	$8.3 \cdot 10^{-6}\ s$
time window	$0.5\ s$

Figure 12. Parameters used for the FD simulations.

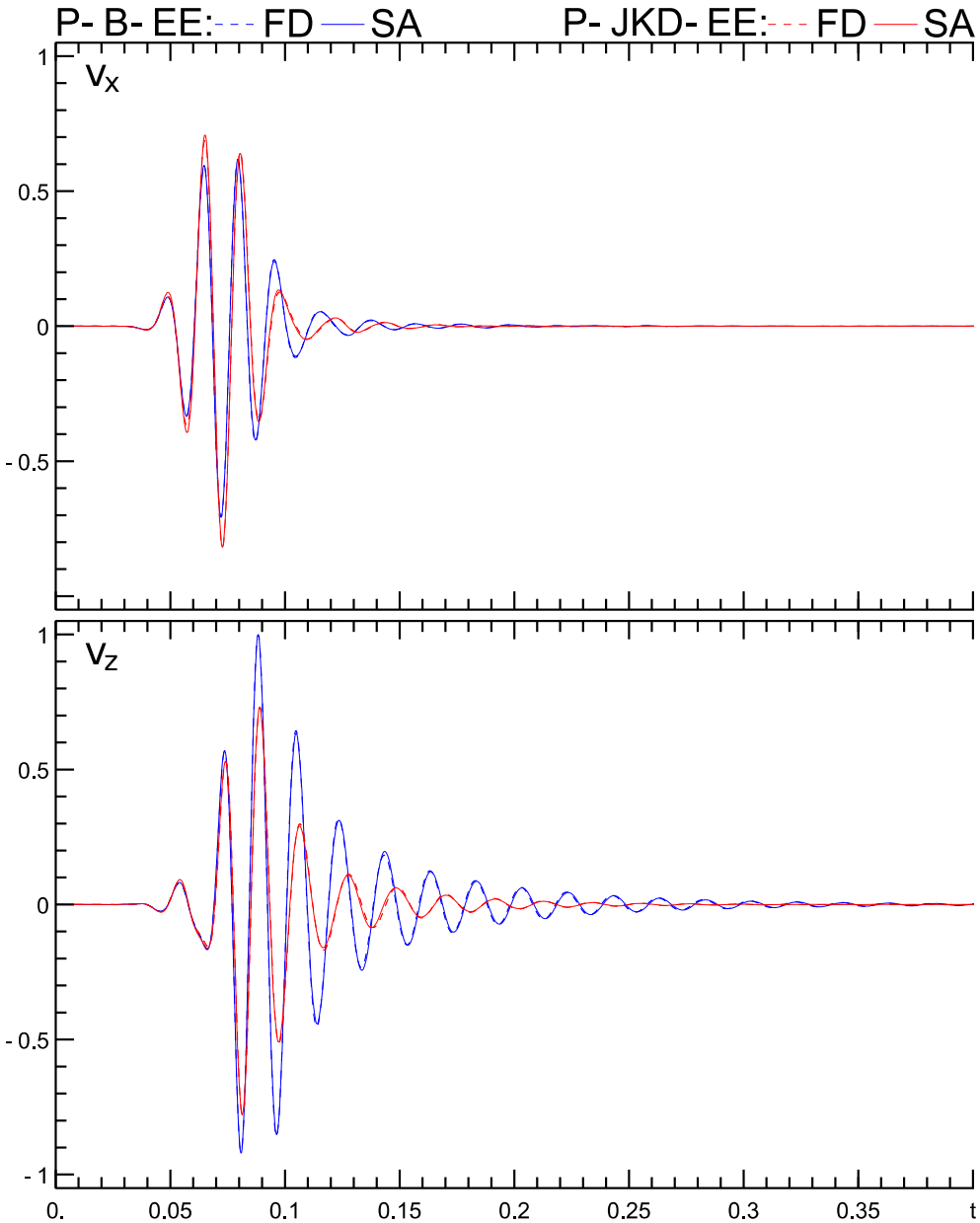

Figure 13. The v_x and v_z seismograms at receiver R1 in the model of the poroelastic layer over the elastic layer and half-space. P-B-EE and P-JKD-EE denote models with Biot's constant resistive friction and JKD frequency-dependent resistive friction in the upper poroelastic layer, respectively. FD seismograms are compared with seismograms calculated by the SA method.

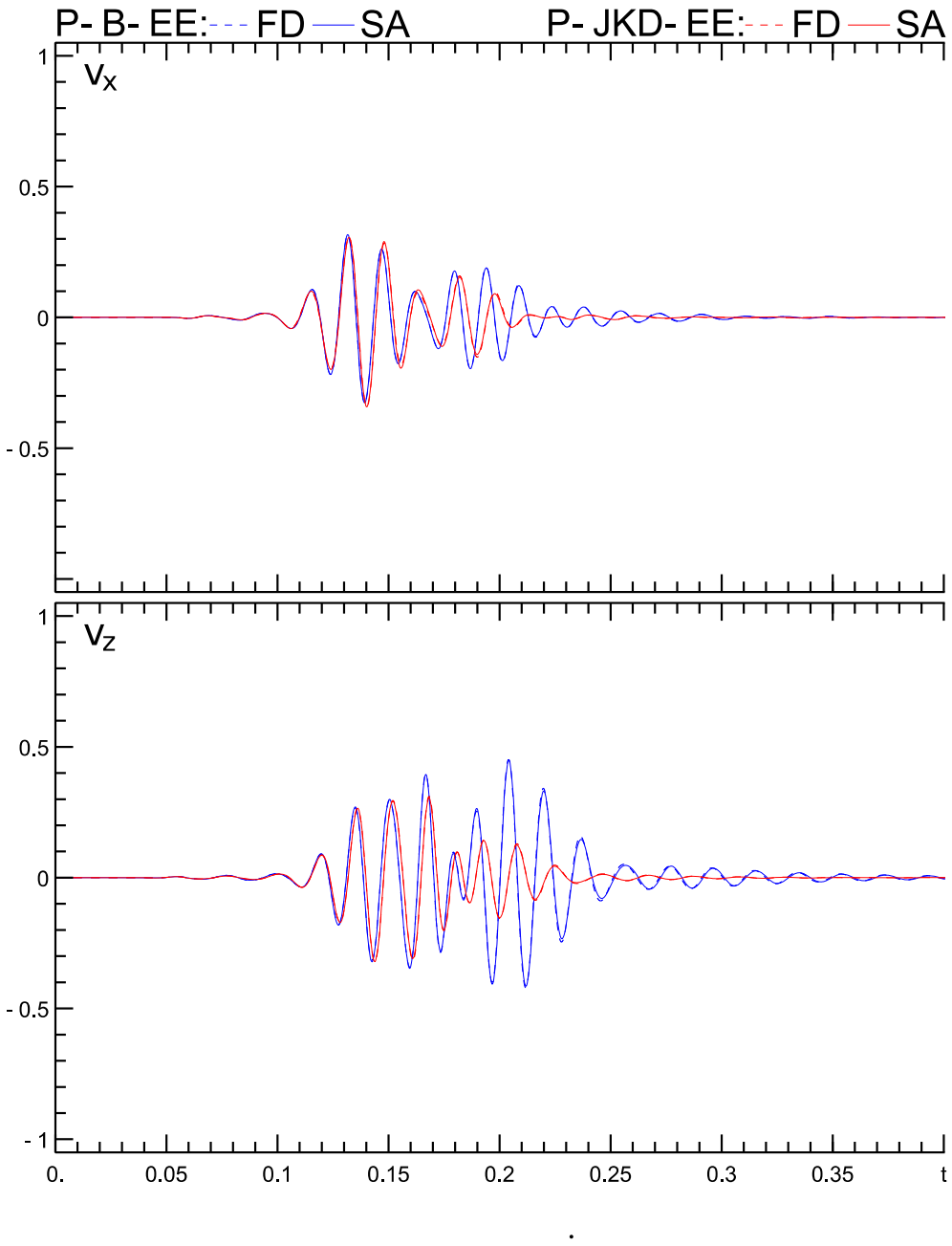

Figure 14. The same as in Fig. 13, but for receiver R2.

Relations (45) may be written as

$$\varepsilon_{xx}^{E} = \frac{1}{\Lambda^{E}}\sigma_{xx} - \frac{\lambda^{E}}{\Lambda^{E}}\varepsilon_{zz}$$
$$\varepsilon_{xx}^{P} = \frac{1}{\Lambda^{P}}\sigma_{xx} - \frac{\lambda^{P}}{\Lambda^{P}}\varepsilon_{zz} + \frac{\alpha^{P}}{\Lambda^{P}}\, p^{P} \tag{46}$$

Continuity of σ_{xx}, ε_{zz} and p, and the arithmetic averaging of ε_{xx}^{E} and ε_{xx}^{P} lead to

$$\langle \varepsilon_{xx} \rangle^{x} = \left(\langle \Lambda \rangle^{Hx}\right)^{-1} \sigma_{xx} - \left\langle \frac{\lambda}{\Lambda} \right\rangle^{x} \varepsilon_{zz} + \left\langle \frac{\alpha}{\Lambda} \right\rangle^{x} p^{P} \tag{47}$$

and we obtain for the stress component

$$\sigma_{xx} = \langle \Lambda \rangle^{Hx} \langle \varepsilon_{xx} \rangle^{x} + \left\langle \frac{\lambda}{\Lambda} \right\rangle^{x} \langle \Lambda \rangle^{Hx} \varepsilon_{zz} - \left\langle \frac{\alpha}{\Lambda} \right\rangle^{x} \langle \Lambda \rangle^{Hx} p^{P} \tag{48}$$

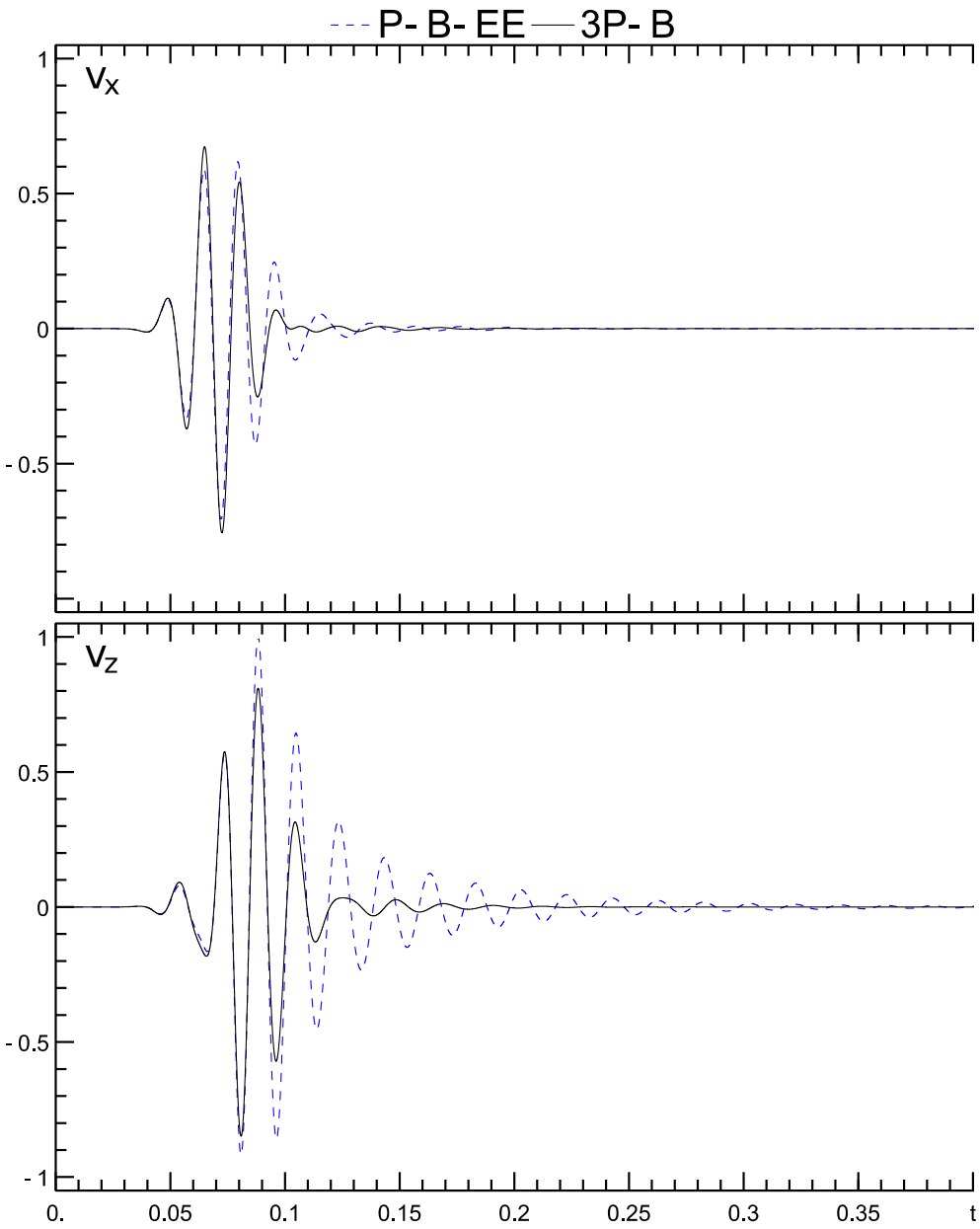

Figure 15. The FD v_x and v_z seismograms at receiver R1 in the model of the poroelastic layer over the elastic layer and half-space P-B-EE compared with those for the model of two poroelastic layers over the poroelastic half-space 3P-B. Biot's constant resistive friction in the poroelastic media assumed.

For σ_{zz}, we may write

$$\sigma_{zz}^E = \lambda^E\ \varepsilon_{xx}^E + \Lambda^E \varepsilon_{zz}$$
$$\sigma_{zz}^P = \lambda^P\ \varepsilon_{xx}^P + \Lambda^P \varepsilon_{zz} - \alpha^P p^P \tag{49}$$

Before averaging σ_{zz}^E and σ_{zz}^P we have to express ε_{xx}^E and ε_{xx}^P using continuous field quantities. Using eq. (46) in eq. (49) we obtain

$$\sigma_{zz}^E = \frac{\lambda^E}{\Lambda^E}\sigma_{xx} + \left(\Lambda^E - \frac{\lambda^E\lambda^E}{\Lambda^E}\right)\varepsilon_{zz}$$
$$\sigma_{zz}^P = \frac{\lambda^P}{\Lambda^P}\sigma_{xx} + \left(\Lambda^P - \frac{\lambda^P\lambda^P}{\Lambda^P}\right)\varepsilon_{zz} - \left(\alpha^P - \frac{\alpha^P\lambda^P}{\Lambda^P}\right)\ p^P \tag{50}$$

Continuity of σ_{xx}, ε_{zz} and the arithmetic averaging of σ_{zz}^E and σ_{zz}^P lead to

$$\langle\sigma_{zz}\rangle^x = \left\langle\frac{\lambda}{\Lambda}\right\rangle^x \sigma_{xx} + \left\langle\Lambda - \frac{\lambda^2}{\Lambda}\right\rangle^x \varepsilon_{zz} - \left\langle\alpha - \frac{\alpha\,\lambda}{\Lambda}\right\rangle^x\ p^P \tag{51}$$

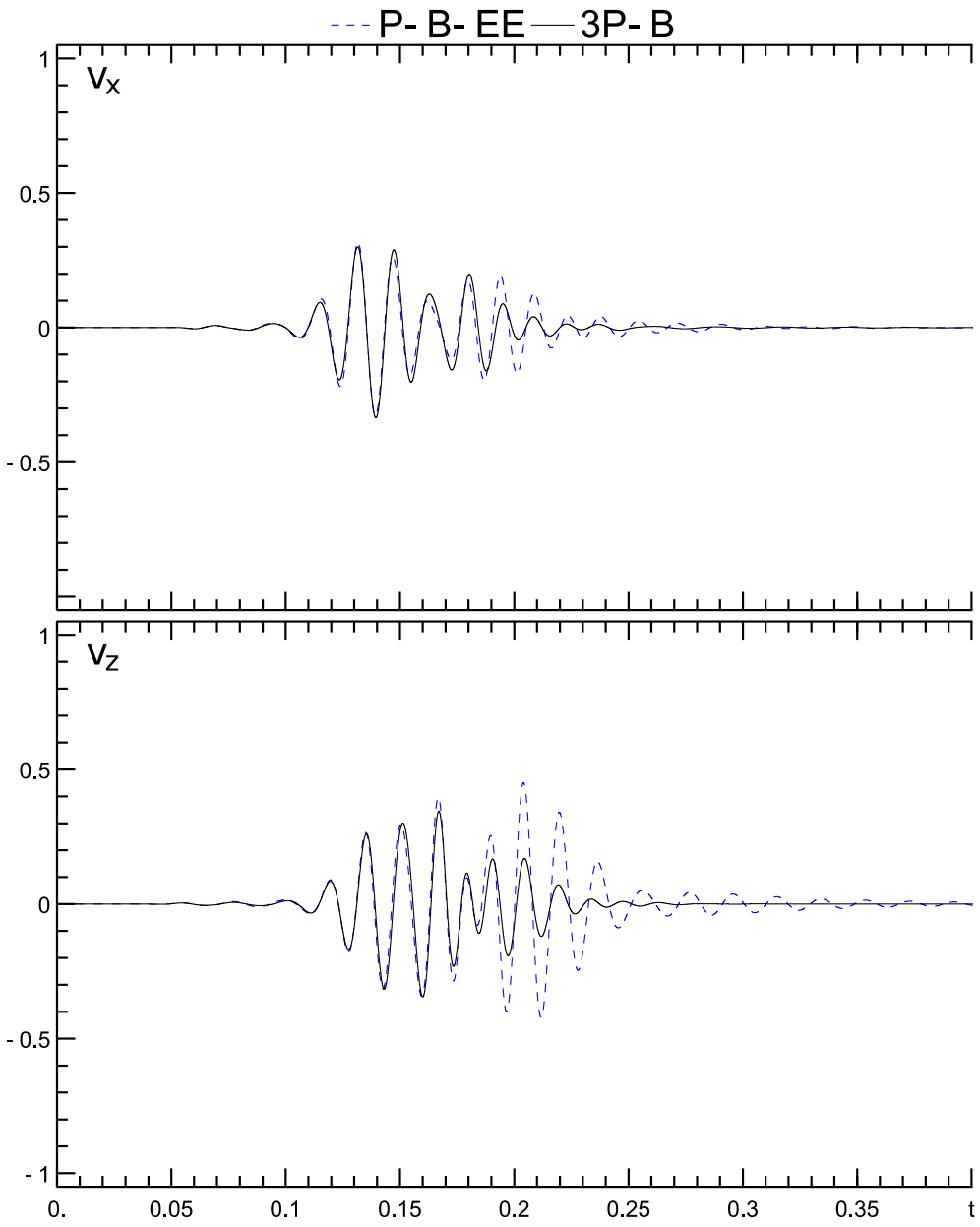

Figure 16. The same as in Fig. 15, but for receiver R2.

Substituting the right-hand side of eq. (48) for σ_{xx} gives the final relation for σ_{zz}:

$$\begin{aligned}\langle\sigma_{zz}\rangle^x = &\left\langle\frac{\lambda}{\Lambda}\right\rangle^x \langle\Lambda\rangle^{Hx}\langle\varepsilon_{xx}\rangle^x \\ &+\left[\left\langle\Lambda-\frac{\lambda^2}{\Lambda}\right\rangle^x+\left(\left\langle\frac{\lambda}{\Lambda}\right\rangle^x\right)^2\langle\Lambda\rangle^{Hx}\right]\varepsilon_{zz} \\ &-\left(\left\langle\alpha-\frac{\lambda\,\alpha}{\Lambda}\right\rangle^x+\left\langle\frac{\alpha}{\Lambda}\right\rangle^x\left\langle\frac{\lambda}{\Lambda}\right\rangle^x\langle\Lambda\rangle^{Hx}\right)p^P\end{aligned} \tag{52}$$

5.3.3 Fluid pore pressure at a planar interface perpendicular to the x-axis

Recall the boundary condition:

$$-p^P=\sigma_{xx}^E \tag{53}$$

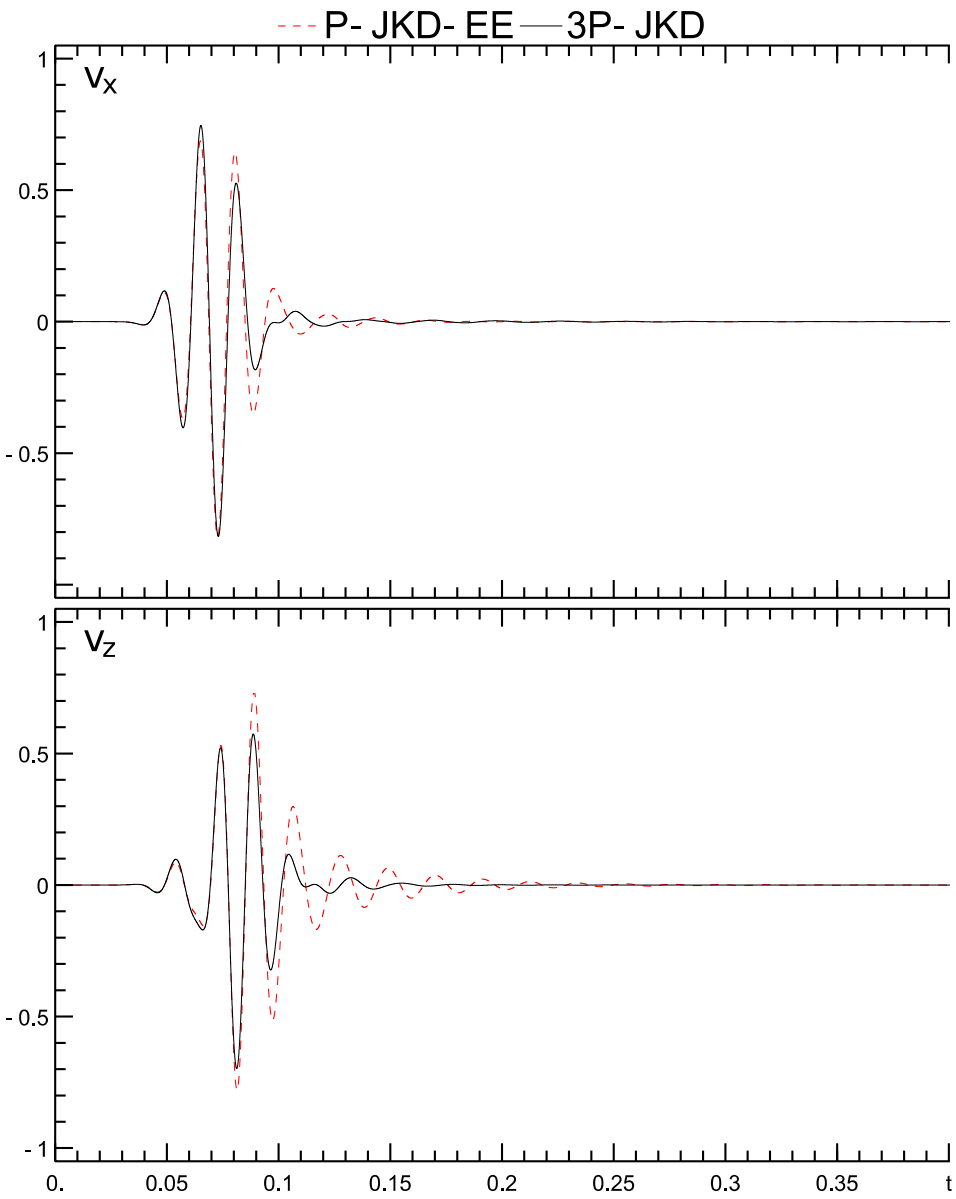

Figure 17. The FD v_x and v_z seismograms at receiver R1 in the model of the poroelastic layer over the elastic layer and half-space P-JKD-EE compared with those for the model of two poroelastic layers over the poroelastic half-space 3P-JKD. JKD frequency-dependent resistive friction in the poroelastic media assumed.

For two half-spaces in contact we may write

$$\sigma_{xx}^E = \Lambda^E\, \varepsilon_{xx}^E + \lambda^E \varepsilon_{zz}$$
$$p^P = -\alpha^P M^P \varepsilon_{xx}^P - \alpha^P M^P \varepsilon_{zz} - M^P \varepsilon_w^P \tag{54}$$

The boundary condition (53) and notation $p = p^P = -\sigma_{xx}^E$ imply

$$p = -\Lambda^E\, \varepsilon_{xx}^E - \lambda^E \varepsilon_{zz}$$
$$p = -\alpha^P M^P \varepsilon_{xx}^P - \alpha^P M^P \varepsilon_{zz} - M^P \varepsilon_w^P \tag{55}$$

Using eq. (46) for expressing ε_{xx}^E and ε_{xx}^P in terms of the continuous field variables we obtain

$$p = -\sigma_{xx}\left(1 + M^P \frac{\alpha^P \alpha^P}{\Lambda^P}\right) p = -\alpha^P M^P \frac{1}{\Lambda^P}\sigma_{xx} - \alpha^P M^P \left(1 - \frac{\lambda^P}{\Lambda^P}\right)\varepsilon_{zz} - M^P \varepsilon_w^P \tag{56}$$

The first equation is just the boundary condition. The second of the equations may be written as

$$\varepsilon_w^P = -\frac{\alpha^P}{\Lambda^P}\sigma_{xx} - \left(\alpha^P - \frac{\alpha^P \lambda^P}{\Lambda^P}\right)\varepsilon_{zz} - \left(\frac{1}{M^P} + \frac{\alpha^P \alpha^P}{\Lambda^P}\right) p \tag{57}$$

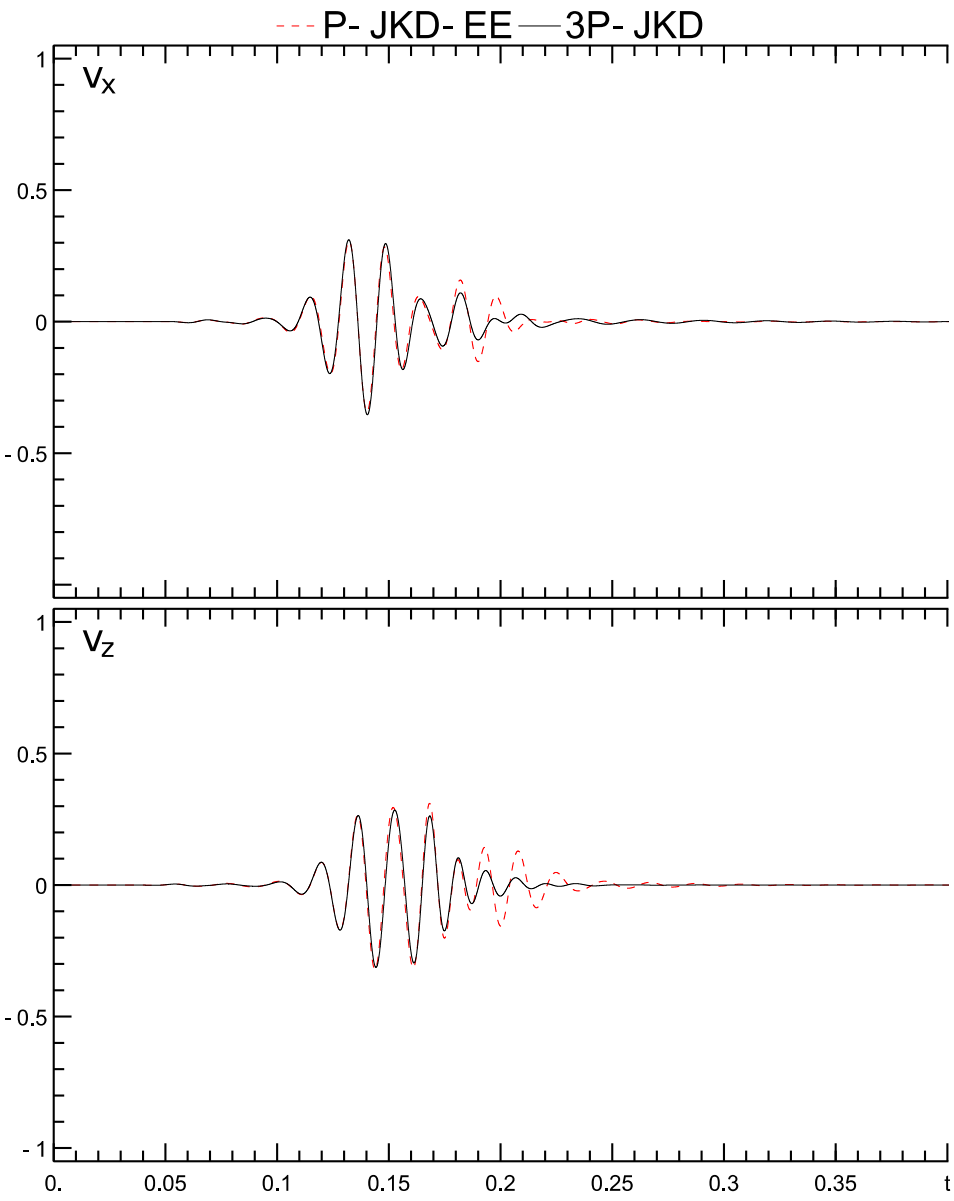

Figure 18. The same as in Fig. 17, but for receiver R2.

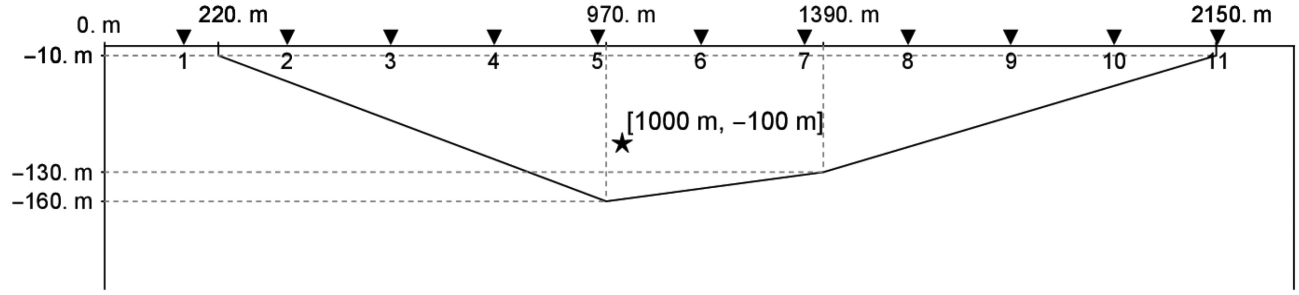

Figure 19. Geometry of the sediment–bedrock interface in the simplified model of the sedimentary basin. Sediments are water-saturated up to the free surface. Black triangles indicate positions the selected receivers. Star indicates position of the source. The horizontal-to-vertical scale is 1:2, values along the horizontal and vertical axes are in m. Material parameters are shown in Fig. 20.

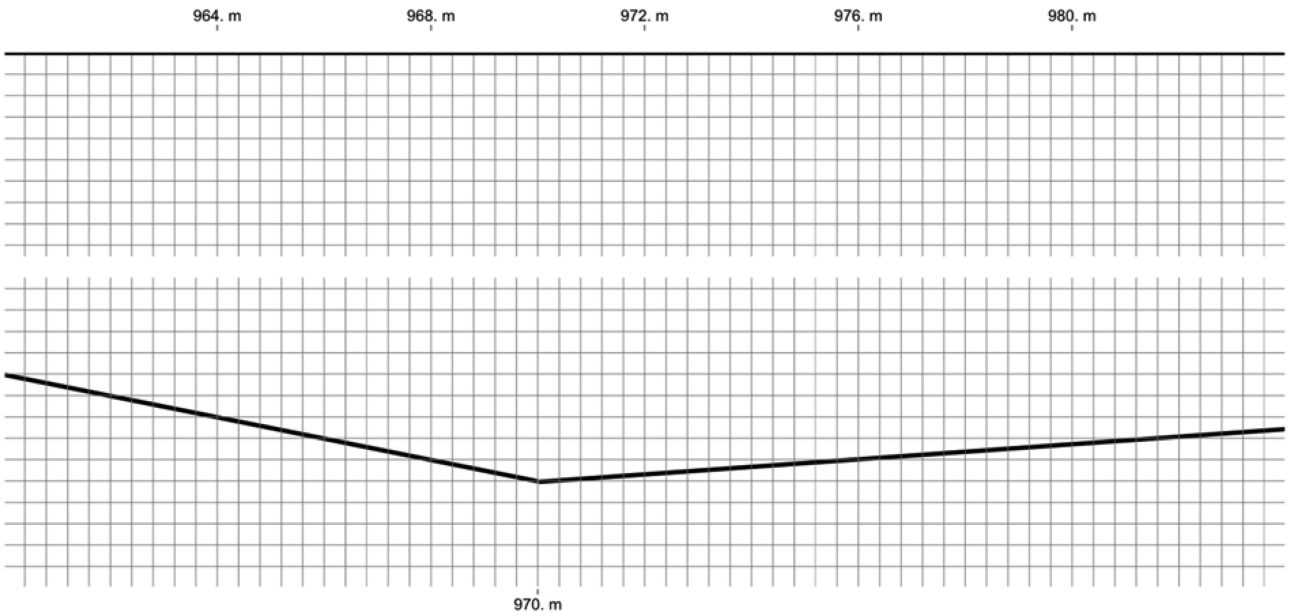

Figure 20. The deepest part of the sediment–bedrock interface in the simplified model of the sedimentary basin (shown in Fig. 19) in the uniform spatial FD grid. The sediment–bedrock interface does not follow grid lines.

Application of averaging gives

$$\langle \varepsilon_w \rangle^x = -\left\langle \frac{\alpha}{\Lambda} \right\rangle^x \sigma_{xx} - \left\langle \alpha - \frac{\alpha\,\lambda}{\Lambda} \right\rangle^x \varepsilon_{zz} - \left\langle \frac{1}{M} + \frac{\alpha\,\alpha}{\Lambda} \right\rangle^x p \tag{58}$$

Substitution of σ_{xx} by the right-hand side of eq. (48) and rearrangement leads eventually to

$$\begin{aligned} p = & -\frac{1}{\left\langle \frac{1}{M} + \frac{\alpha^2}{\Lambda} \right\rangle^x - \left(\left\langle \frac{\alpha}{\Lambda} \right\rangle^x \right)^2 \langle \Lambda \rangle^{Hx}} \\ & \times \left[\left\langle \frac{\alpha}{\Lambda} \right\rangle^x \langle \Lambda \rangle^{Hx} \langle \varepsilon_{xx} \rangle^x \right. \\ & + \left(\left\langle \alpha - \frac{\alpha\,\lambda}{\Lambda} \right\rangle^x + \left\langle \frac{\alpha}{\Lambda} \right\rangle^x \left\langle \frac{\lambda}{\Lambda} \right\rangle^x \langle \Lambda \rangle^{Hx} \right) \varepsilon_{zz} \\ & \left. + \langle \varepsilon_w \rangle^x \right] \end{aligned} \tag{59}$$

Analogously, we could derive the averaging formulae also for a planar interface perpendicular to the z-axis. Then, we can proceed using the same considerations that we presented in the paper by Moczo *et al.* (2019). Eventually, the averaging procedure leads formally to the same averaging formulae as in the case of the poroelastic medium—matrix (A3) in this paper.

5.3.4 Notes on the evaluation of the averaged parameters

We need to look at the averaged parameters in case when they include averaging over the elastic part(s). That is, over parts with parameters $\alpha^E = 0$, $m^E \to \infty$ and $M^E \to \infty$.

Before we continue, let us note that the averaged material parameters are calculated in a grid-model-preparation computer code producing a grid-model file. The file contains all averaged grid material parameters appearing in matrices T_{pq}, X_{pq}, Z_{pq} and S_{pq}. The matrices then enter an FD scheme in another computer code for computing wavefield.

Look first at the averaged parameters XX, ZZ, XZ, XP and ZP appearing in the constitutive relations (24) and consequently also in matrices T_{pq}, X_{pq}, Z_{pq} and S_{pq} in the unified matrix-form equation (30) that incorporates relations (24). We can immediately see that evaluation of XX, ZZ, XZ, XP and ZP poses no problem—no matter what the composition of the grid cell is.

Parameter Ψ appearing in the denominator in matrices X_{pq} and Z_{pq}, is non-zero,$\Psi \neq 0$, if the grid cell is fully poroelastic or mixed. In case of a fully elastic grid cell, $\Psi^E = 0$ due to $1/M^E = 0$ and $\alpha^E = 0$. This, however, does not pose a problem because there is no need to calculate pore pressure p in the elastic medium.

Symbol	Units	Value
sedimentary basin		
solid phase		
ρ_s	kg/m^3	2644
K_s	Pa	$37\cdot10^9$
fluid phase		
ρ_f	kg/m^3	1000
K_f	Pa	$2.25\cdot10^9$
η	$Pa\,s$	$1\cdot10^{-3}$
solid matrix (drained)		
K_m	Pa	$7\cdot10^9$
μ	Pa	$0.792\cdot10^9$
λ_m	Pa	$6.472\cdot10^9$
ϕ		0.27
T		2.3
κ_0	m^2	10^{-10}
saturated porous medium (undrained)		
λ_c	Pa	$3.53\cdot10^9$
b	$Pa\,s\,m^{-2}$	10^7
f_c	Hz	187
velocities		
$VP_{fast}^{\inf}$	m/s	2425
$VP_{slow}^{\inf}$	m/s	757
$VS^{\inf}$	m/s	617
elastic bedrock		
ρ	kg/m^3	2500
K	Pa	$32.5\cdot10^9$
μ	Pa	$5.625\cdot10^9$
λ	Pa	$28.75\cdot10^9$
VP	m/s	4000
VS	m/s	1500

Figure 21. Material parameters and limit values of velocities of the fast *P*, slow *P* and *S* waves. The model of the sedimentary basin is shown in Fig. 19.

5.4 Averaging of material parameters in the equations of motion and additional equations

Similarly as in the case of the constitutive law, the averaging procedure according to Moczo *et al.* (2019) leads formally to the same averaging formulae as in the case of the poroelastic medium—matrix (A4) in this paper.

As in the previous subsection, we need to look at the averaged parameters in the equations of motion (A2), (A4) and (A12), and in the additional equations for the diffusive memory variables (A5)–(A7), in case when they include averaging over the elastic part(s) with parameters $\alpha^E = 0$, $m^E \to \infty$ and $M^E \to \infty$.

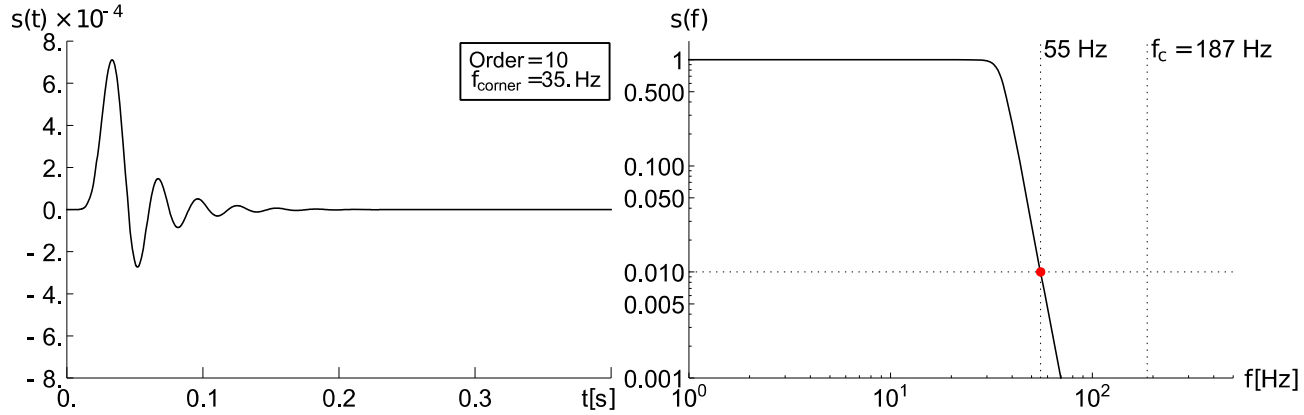

Figure 22. The source time function, its normalized amplitude log–log Fourier spectrum and Biot's characteristic frequency in the poroelastic sediments. The model is shown in Fig. 19.

FD		SE	
size	$3251 \times 1250 = 4\,063\,750$	number of elements	445 517
grid spacing	$0.8m$	number of GLL points	7 137 105
		element size	$0.54 - 21m$
PML zone	100	PML zone	100
time step	$10^{-4}\ s$	time step	$5 \cdot 10^{-6}\ s$
time window $2s$			

Figure 23. Parameters used for the FD and SE simulations. In the SE simulation on the unstructured grid, Lagrange polynomials of degree 4 are used, leading to five GLL integration points irregularly spaced in both directions x and z, and 25 GLL points in one element.

For any type of material in an averaging area, parameters F^{ξ}, P^{ξ} and R^{ξ} are non-zero. Parameters G^{ξ}, H^{ξ} and Q^{ξ} are non-zero in the fully poroelastic averaging area. They are all zero in the fully elastic or mixed averaging area due to $m^E \to \infty$. Parameters G^{ξ} and H^{ξ} always appear in the nominator in the arithmetic averaging in the complementary axis direction. Parameter Q^{ξ} appears in the arithmetic averaging in the complementary axis direction in evaluation of parameters $\langle S^x \rangle^z$ and $\langle S^z \rangle^x$ which are in the denominator in matrices X_{pq}, Z_{pq} and S_{pq}. However, $\langle S^x \rangle^z$ and $\langle S^z \rangle^x$ are always nonzero due to non-zero parameters P^x and P^z.

Given the above consideration, it will be reasonable to describe the medium by $1/m$ with the mass coupling coefficient m being either m^P or m^E.

5.5 Classification of material parameters

The above considerations on averaged material parameters appearing in the constitutive relations, equation of motions and additional equations for the diffusive memory variables are summarized in Fig. 4 that shows which averaged parameters are non-zero, zero or set equal to zero in three possible cases for an averaging area: fully elastic, fully poroelastic and mixed.

The main important conclusion of this section is: the averaging of the strongly poroelastic medium is applicable also to a medium composed of the poroelastic and strictly elastic parts.

The purely poroelastic medium could be specified by the following spatially dependent material parameters:

$$\lambda, \mu, \Lambda, \alpha, M, \rho_f, \rho, m, b, \Omega \tag{60}$$

Values of the above parameters are used for evaluating the averaged parameters appearing in matrices $\mathbf{S}_A$, $\mathbf{R}_A$, $\mathbf{D}_A$ and $\mathbf{\Omega}_A$, and then, consequently, in matrices T_{pq}, X_{pq}, Z_{pq}, and S_{pq}.

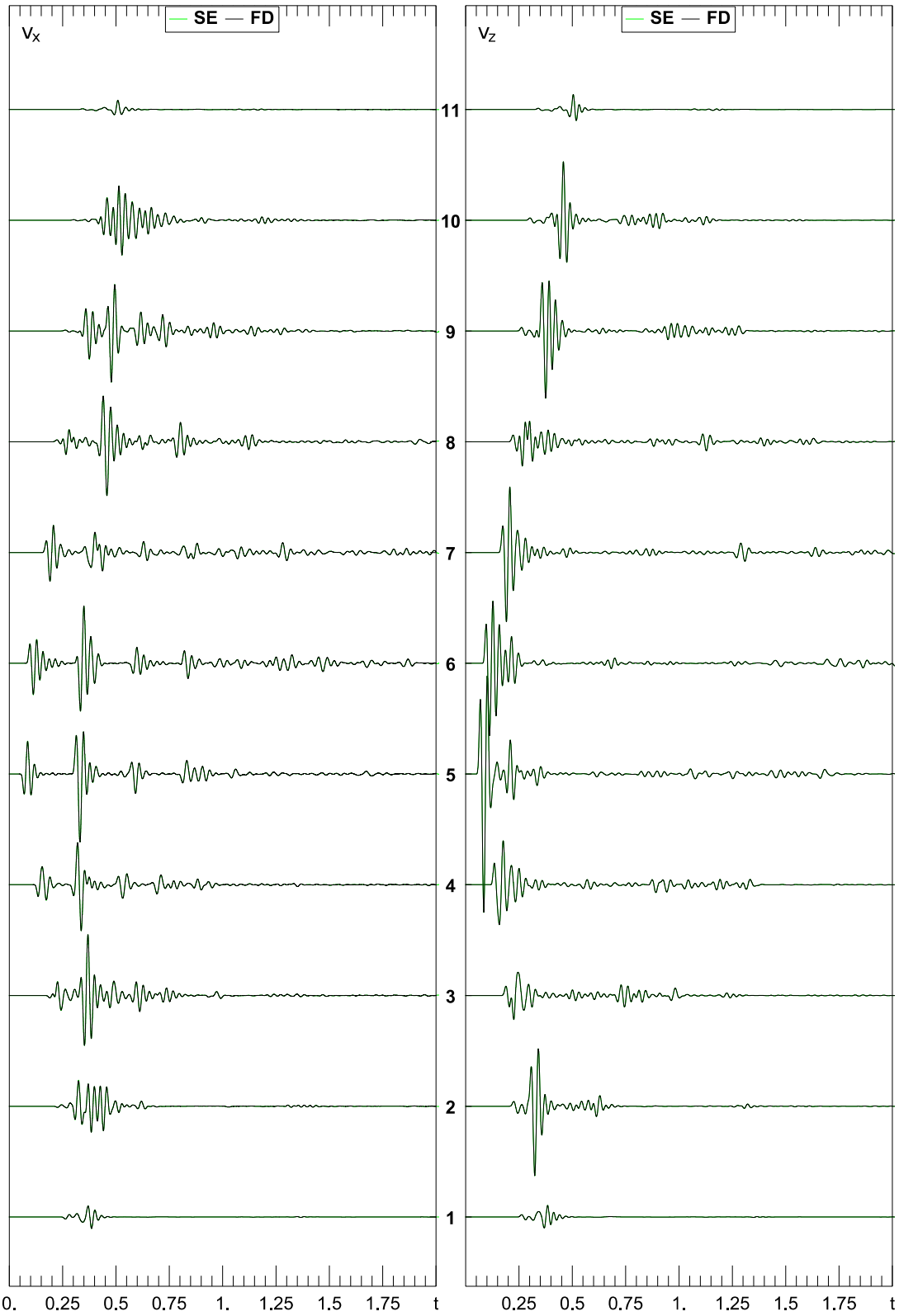

Figure 24. Comparison of the FD and SE seismograms at three selected receivers at the free surface of the poroelastic sedimentary basin embedded in the elastic bedrock. Receivers v_z 1 and v_x 1 are at [148.0,0.0] and [147.6, −0.4], respectively. Distances between neighbouring receivers are 200 m.

Considering the infinite values of M and m in the elastic parts, the medium composed of the poroelastic and elastic parts may be specified by the following spatially dependent material parameters:

$$\lambda, \mu, \Lambda, \alpha, 1/M, \rho_f, \rho, 1/m, b, \Omega \tag{61}$$

In the latter list of the input material parameters, $\alpha = 0$, $1/M = 0$, $1/m = 0$, $\rho_f = \rho$, $b = 0$ and $\Omega = 0$ are used for the elastic parts.

6 UPDATING WAVEFIELD USING A FINITE-DIFFERENCE SCHEME

As explained above, the averaged parameters account for presence of the poroelastic and elastic parts by approximating boundary conditions at the P/P, P/E and E/Ematerial interfaces. The interfaces can have an arbitrary shape and position in the grid. The averaged material parameters also account for smooth heterogeneity inside layers or block. As said before, the averaged material parameters at the appropriate grid positions are calculated in the grid-model-preparation computer code. The output file of the code becomes an input for the code realizing calculation of wavefield using the FD scheme. The wavefield is described by wavefield variables $\{ VX, VZ, QX, QZ, TXX, TZZ, TXZ, FP, \psi_l^x, \psi_l^z \}$; $l = 1, ..., N$. We will use symbol Φ to refer to any of the wavefield variables. The FD scheme is given in Appendix D. The grid cell is shown in Fig. A1.

6.1 Medium consisting of the JKD poroelastic and elastic parts

Here, we consider the use of one FD scheme (formally for the poroelastic medium) for the medium consisting of the poroelastic and strictly elastic parts. We assume the JKD frequency-dependent resistive friction in the poroelastic parts. The JKD resistive friction is easily formally reduced to the Biot's model of the constant resistive friction or zero resistive friction. This means that the scheme makes it possible to consider a model of medium in which there are poroelastic parts with JKD resistive friction and parts with zero or constant resistive friction.

Let us emphasize again that the use of the scheme formally for the poroelastic medium does not mean that the elastic parts are poroelastic with effectively elastic behaviour. The elastic parts of the model are in our approach strictly elastic.

An FD scheme for updating a field variable needs values of field variables and effective (averaged) material parameters at a set of neighbouring gridpoints. This set is called a grid stencil.

In what follows we show that the FD scheme for the poroelastic medium can be used for the medium consisting of the poroelastic and strictly elastic parts without additional logical branching (i.e. without using IF conditions).

Grid stencil fully in the poroelastic medium

This is the standard situation for the FD scheme, all field variables and material parameters are available.

Grid stencil fully in the elastic medium

Neither this situation poses a problem. The FD scheme can be used without any additional logical branching (using IF conditions). This is because at the corresponding gridpoints averaged material parameters XP/Ψ, ZP/Ψ, $1/\Psi$ are set equal to zero, and

$\langle G^x \rangle^z$, $\langle G^z \rangle^x$, $\langle G^x/R^x \rangle^z$, $\langle G^z/R^z \rangle^x$ and $\tilde{s}_{q_x}^{v_x}$, $\tilde{s}_{q_x}^{\psi_n^x}$, $\tilde{s}_{\psi_n^x}^{v_x}$, $\tilde{s}_{\psi_n^x}^{q_x}$, $\tilde{s}_{\psi_n^x}^{\psi_l^x}$, $\tilde{s}_{q_z}^{v_z}$, $\tilde{s}_{q_z}^{\psi_n^z}$, $\tilde{s}_{\psi_n^z}^{v_z}$, $\tilde{s}_{\psi_n^z}^{q_z}$, $\tilde{s}_{\psi_n^z}^{\psi_l^z}$ are evaluated as zero in the grid-model-preparation code. As a consequence, at the corresponding gridpoint, fluid pore pressure FP, particle velocities QX, QZ, diffusive memory variables ψ_n^x, ψ_n^z, and auxiliary field variables $QX*$, $QZ*$, ψ_n^{x*}, ψ_n^{z*} are all evaluated as zero.

Gridpoint of the updated field variable $\Phi 1$ in the poroelastic medium, stencil requiring value of field variable $\Phi 2$ *at a gridpoint in the elastic medium*

The updating of the particle velocities VX, VZ, QX, QZ and diffusive memory variables ψ_n^x, ψ_n^z may formally require value of the fluid pore pressure FP in the elastic medium. That is formally zero. The updating of fluid pore pressure FP requires values of the particle velocities QX, QZ in the elastic medium. These are formally zero.

Gridpoint of the updated variable $\Phi 1$ *in the elastic medium, stencil requiring value of variable* $\Phi 2$ *at a gridpoint in the poroelastic medium*

The updating of all wavefield variables in the elastic medium has all variables located in the poroelastic medium available.

Gridpoint of the updated variable $\Phi 1$ *at the interface between the poroelastic and elastic media.*

Depending on which particle-velocity component and corresponding diffusive memory variable are located at the gridpoint at the interface, either averaged material parameters $\langle G^x \rangle^z$, $\langle G^x/R^x \rangle^z$, $\tilde{s}_{q_x}^{v_x}$, $\tilde{s}_{q_x}^{\psi_n^x}$, $\tilde{s}_{\psi_n^x}^{v_x}$, $\tilde{s}_{\psi_n^x}^{q_x}$, $\tilde{s}_{\psi_n^x}^{\psi_l^x}$ or averaged material parameters $\langle G^z \rangle^x$, $\langle G^z/R^z \rangle^x$, $\tilde{s}_{q_z}^{v_z}$, $\tilde{s}_{q_z}^{\psi_n^z}$, $\tilde{s}_{\psi_n^z}^{v_z}$, $\tilde{s}_{\psi_n^z}^{q_z}$, $\tilde{s}_{\psi_n^z}^{\psi_l^z}$ are zero, and, as a consequence, either wavefield variables QX, QX^*, ψ_n^x, ψ_n^{x*} or wavefield variables QZ, QZ^*, ψ_n^z, ψ_n^{z*} are zero, respectively.

6.2 Medium consisting of the poroelastic parts with zero or constant resistive friction and elastic parts

Here, we consider the use of one poroelastic FD scheme if all poroelastic parts have only zero or constant resistive friction. In this case, there are no diffusive memory variables ψ_n^x, ψ_n^z and auxiliary field variables ψ_n^{x*}, ψ_n^{z*}. Therefore, it is computationally considerably more efficient to use an alternative computer code based on the FD scheme for the poroelastic medium without diffusive memory variables and auxiliary variables. Such scheme was presented by Moczo *et al.* (2019).

7 NUMERICAL TESTS

We present numerical tests of our discrete representation of the strongly heterogeneous medium composed of poroelastic and elastic parts as well as our FD scheme based on the representation. In tests against the analytical and semi-analytical solutions we must consider canonical models, while a more complex geometry is tested against the independent numerical method.

In the first test, we compare FD seismograms with seismograms calculated using the A and SE methods. The A method was developed by Diaz & Ezziani (2008, 2010). The SE method was developed by Morency & Tromp (2008) and implemented in the open source software SPECFEM2D (e.g. Komatitsch & Vilotte 1998) used for the SE calculations.

In the second test, we compare FD seismograms with those calculated using the SA method developed by Mesgouez & Lefeuve-Mesgouez (2009) and Lefeuve-Mesgouez *et al.* (2012).

In the third test, we compare FD seismograms with those calculated by the SE method in a simplified sedimentary basin model. This test also demonstrates a sub-cell resolution of our FD scheme.

7.1 Model of two half-spaces

Geometry of the model, positions of the source (indicated by a star) and two receivers (P1 and P2) are shown in the upper panel of Fig. 5. Recall that each of the two receivers is split in the v_x and v_z parts due to the staggered grid. Material parameters of the half-spaces are shown in Fig. 6. The upper poroelastic half-space with a zero resistive friction (zero viscosity) is in the horizontal planar contact with the lower perfectly elastic half-space. We test in this case the simplest possible configuration of the P/E interface. The model and the source are the same as in Morency & Tromp (2008, Fig. 13). The difference is in the source and receiver positions. An explosive source (line source perpendicular to the plane of the wavefield propagation) is acting in the upper poroelastic half-space. The source is applied to both the solid matrix and fluid through the stress and pressure increments in the constitutive laws for stress and pressure, respectively. The source-time function is given by wavelet

$$s(t) = 2\,\beta\left[1 + 2\,\beta(t - t_S)^2\right]\exp\left[\beta\,(t - t_S)^2\right]; \qquad \beta = -(\pi\, f_P)^2 \tag{62}$$

The values of the free parameters t_P and t_S, amplitude Fourier spectrum and a log–log spectrum of the wavelet are shown in Fig. 5. The P/E interface coincides with the grid line going through positions of the v_z, q_z and σ_{xz}. Computational parameters used in the FD and SE simulations are shown in Fig. 7. Considering $VP^{\inf}_{slow} = 1186\,\mathrm{m\,s^{-1}}$ and the chosen maximum frequency $f_{\max} = 41.45\,\mathrm{Hz}$, the corresponding minimum wavelength 28.61 m is sampled by 7.15 grid spacings.

Fig. 8 shows the v_x and v_z seismograms at receivers P1 and P2 in the model of the two half-spaces with the P/E interface obtained using the A, SE and our FD methods. In order to quantitatively characterize differences between the FD and A seismograms, and between the FD and SE seismograms, we evaluated the time–frequency envelope and phase misfits—TFEM and TFPM (Kristekova *et al.* 2006, 2008, 2009). We can see small misfits close to the maximum frequency but mainly very low misfits at and close to the dominant frequency of 15 Hz. The level of agreement is a good basis for comparing the SE and FD solutions for a more complicated model of a sedimentary basin in Section 7.3.

7.2 Model of two horizontal layers over half-space

Geometry of the model, positions of the source and two receivers (R1 and R2) are shown in the upper panel of Fig. 9. We consider four rheological variants of the model:

3P-B	both layers and the half-space are poroelastic, Biot's constant resistive friction assumed
3P-JKD	both layers and the half-space are poroelastic, JKD frequency-dependent permeability and resistive friction assumed
P-B-EE	poroelastic upper layer over an elastic layer and elastic half-space, Biot's constant resistive friction assumed in the upper layer
P-JKD-EE	poroelastic upper layer over an elastic layer and elastic half-space, JKD frequency-dependent permeability and resistive friction assumed in the upper layer

Material parameters of the 3P-B and 3P-JKD models are in Fig. 10, those of the P-B-EE and P-JKD-EE models in Fig. 11.

This set of the canonical models makes it possible to

A single vertical force (a line source perpendicular to the plane of wavefield propagation) is acting at the free surface and applied to both the solid matrix and fluid through the body-force terms in the equations of motion for the v_z and q_z components of the solid-matrix and relative fluid particle velocities. The source-time function is given by Ricker wavelet

$$s(t) = \frac{\sqrt{\pi}}{2}\left(a - \frac{1}{2}\right)e^{-a}; \qquad a = \left(\pi\,\frac{t - t_S}{t_P}\right)^2 \tag{63}$$

The values of the free parameters t_P and t_S, and values of the Biot's characteristic frequency f_c in the upper poroelastic layer are shown in the bottom panel of Fig. 9. Computational FD parameters are in Fig. 12. Considering $VS = 227.2\,\mathrm{m\,s^{-1}}$ and the chosen maximum

■	Test accuracy of modelling
-	P-B/P-B and P-JKD/P-JKD interfaces,
-	P-B/E and P-JKD/E interfaces,
-	E/E interface
	by one and the same discrete representation and FD scheme.
■	Compare purely poroelastic models with combined poroelastic/elastic models for two variants of resistive friction.

frequency $f_{\max} = 105.6$Hz, the corresponding minimum wavelength 2.15 m is sampled by 23.89 grid spacings. Such dense sampling is not necessary. As in all other cases, three times coarser sampling would give almost the same result. Here, we wanted to meet two criteria together: (i) The two specific layer thicknesses are chosen so that the 1-D vertical resonance frequency in the upper layer is very close to the resonance frequency of both layers together. Such coincidence supports relatively strong interference in the two layers. (2) In this canonical comparison, we wanted to have all interfaces coinciding with the grid lines. Both interfaces coincide with the grid lines going through v_z, q_z and σ_{xz}. Moreover, in the process of detailed checking, we wanted to have the receiver positions as densely as in the second numerical example in paper by Gregor *et al.* (2021), in which we have the same material parameters in the upper layer.

Fig. 13 shows the v_x and v_z seismograms at receiver R1 in the P-B-EE and P-JKD-EE models calculated by the FD and SA methods. The figure shows a very good agreement between the FD and SA seismograms for both model variants—Biot's and JKD in the upper poroelastic layer. As expected, based on results by Gregor *et al.* (2021), there is a considerable difference between seismograms for the Biot's and JKD variants of the upper poroelastic layer. Fig. 14 shows a similar comparison for receiver R2.

Based on the above verification of our representation of the P/E interface, it is interesting to compare both mixed poroelastic/elastic models P-B-EE and P-JKD-EE with their purely poroelastic counterparts 3P-B and 3P-JKD. As explained above, both layers and the half-space are poroelastic in latter models.

Fig. 15 shows the v_x and v_z FD seismograms at receiver R1 in the 3P-B and P-B-EE models. Fig. 16 shows the same at receiver R2. Figs 17 and 18 are analogous to Figs 15 and 16 but compare FD seismograms in the 3P-JKD and P-JKD-EE models. Note that we do not show SA seismograms in Figs 15–18 because for the mixed models they are shown in Figs 13 and 14, and we verified our FD seismograms for purely poroelastic models with those obtained by the SA method in paper by Gregor *et al.* (2021). The purpose of Figs 15–18 is to illustrate effect of replacing the middle poroelastic layer and poroelastic half-space by the elastic layer and elastic half-space, respectively, for both Biot's and JKD variants of resistive friction in the poroelastic media. We can see in the figures that visual differences between the 3P-B and P-B-EE seismograms are clearly larger than the difference between the 3P-JKD and P-JKD-EE seismograms.

7.3 Simplified model of a sedimentary basin

Here, we compare our FD solution with solution by the SE method. We choose a model of a surface sedimentary basin with a simplified geometry shown in Fig. 19. The SE method using domain decomposition, the SE elements follow exactly the shape of the sediment–bedrock interface. This means that the SE simulation exactly accounts for the geometry of the interface and, consequently, the SE seismograms can be considered a sufficiently accurate reference for verifying the FD seismograms. At the same time, the sediment–bedrock interface does not follow grid lines in the uniform spatial FD grid. This is illustrated for the deepest part of the interface in Fig. 20.

Material parameters are shown in Fig. 21. We consider poroelastic sediments with constant resistive friction embedded in an (strictly) elastic bedrock. The wavefield is excited by a line (line perpendicular to the vertical plane of propagation) explosive source. Fig. 22 shows the input signal, its amplitude and log–log Fourier spectra, and value of the Biot's characteristic frequency ($f_c = 187\ Hz$). The source time function was obtained by low-pass filtering a discrete Dirac pulse with a 10-pole (sharp) 1-pass (causal) Butterworth filter with corner frequency of 35 Hz. Computational FD parameters are in Fig. 23. Considering $VP^{\inf}_{slow} = 475.3\,\mathrm{m\,s^{-1}}$ and the chosen maximum frequency $f_{\max} = 55$Hz, the corresponding minimum wavelength 8.64 m is sampled by 10.8 grid spacings. Note that this specific sampling is also due to the comparison procedure and is larger than necessary.

The SE seismograms are calculated using the open-source software SPECFEM2D (e.g. Komatitsch & Vilotte 1998) and the software CUBIT (Blacker *et al.* 1994) to design an unstructured grid, with elements following exactly the interface between the poroelastic and elastic domains. Comparison of the FD and SE seismograms is shown in Fig. 24. The figure shows very good agreement between the FD and SE seismograms. As it is illustrated in Fig. 20, the sediment–bedrock interface in the FD computational model does not follow grid lines. This means, given the very good agreement between the FD and SE seismograms, that the FD scheme is capable of subcell resolution—an interface can have an arbitrary position in the spatial grid.

8 CONCLUSIONS

We have developed a new methodology of the FD modelling of seismic wave propagation in a strongly heterogeneous medium composed of poroelastic (P) and (strictly) elastic (E) parts. A poroelastic part may have either of three models of resistive friction—zero, non-zero constant or JKD frequency-dependent—independently of other poroelastic parts. The model can include P/P, P/E and E/E material interfaces of arbitrary shapes. The medium in between the material interfaces may be smoothly heterogeneous.

A material interface may have an arbitrary position in the spatial grid. This means that our FD scheme has a subcell resolution capability.

Our discrete representation of the strong material heterogeneity is based on averaging of material parameters which approximates boundary conditions at interfaces. Our representation makes it possible to keep computational efficiency of the scheme for a smoothly and weakly heterogeneous medium (i.e. medium without material interfaces).

We have checked accuracy and efficiency of our modelling using numerical tests against independent A, SA and SE methods. In the numerical examples we indicated effect of the P/E interfaces for the poroelastic medium with a constant resistive friction and medium with the JKD model of the frequency-dependent permeability and resistive friction.

We addressed the 2-D *P-SV* problem for the brevity and computational demands. The approach can be, however, readily extended to the 3-D problem.

ACKNOWLEDGEMENTS

This work was supported by the Slovak Research and Development Agency under the contract APVV-15–0560 (project ID-EFFECTS) and by the Slovak Foundation grant VEGA 2/0046/20. Portions of this work were also performed under the auspices of the U.S. Department of Energy by Lawrence Livermore National Laboratory under contract DE-AC52-07NA27344.

We are grateful to Wei Zhang for his constructive criticism, and Associate Editor and an anonymous reviewer for their comments and help.

DATA AVAILABILITY

The data underlying this article will be shared on reasonable request to the corresponding author.

REFERENCES

Alkhimenkov, Y., Khakimova, L. & Podladchikov, Y.Y., 2021a. Stability of discrete schemes of Biot's poroelastic equations, *Geophys. J. Int.,* **225**(1), 354–377.

Alkhimenkov, Y., Räss, L., Khakimova, L., Quintal, B. & Podladchikov, Y., 2021b. Resolving wave propagation in anisotropic poroelastic media using graphical processing units (GPUs), *J. geophys. Res.: Solid Earth,* **126,** e2020JB021175, doi:10.1093/gji/ggaa584.

Berryman, J.G., 1980. Confirmation of Biot's theory, *Appl. Phys. Lett.,* **37**(4), 382–384.

Biot, M.A., 1956. Theory of propagation of elastic waves in a fluid-saturated porous solid. I. Low-frequency range, *J. Acoust. Soc. Am.,* **28**(2), 168–178.

Blacker, T., Bohnhoff, W. & Edwards, T.L., 1994. *CUBIT Mesh Generation Environment. Volume 1: Users Manual.* Sandia National Laboratory, Albuquerque, NM, USA.

Blanc, E., 2013. *Time-Domain Numerical Modeling of Poroelastic Waves: The Biot-JKD Model with Fractional Derivatives, Thèse*, Aix-Marseille Université, pp. 157.

Bourbié, T., Coussy, O. & Zinszner, B., 1987. *Acoustics of Porous Media,* Editions Technip.

Carcione, J.M. & Quiroga-Goode, G., 1995. Some aspects of the physics and numerical modelling of Biot compressional waves, *J. Comput. Acoust.,* **3**(4), 261–280.

Chen, W., Xia, T., Chen, W. & Zhai, C., 2012. Propagation of plane P-waves at interface between elastic solid and unsaturated poroelastic medium, *Appl. Math. Mech. Engl. Ed.,* **33**(7), 829–844.

Cheng, S., Mao, W., Zhang, Q. & Xu, Q., 2021. Wave propagation in the poro-viscoelastic orthorhombic two-phase media: plane-wave theory and wavefield simulation, *Geophys. J. Int.,* **227**(1), 99–122.

de la Cruz, V. & Spanos, T.J.T., 1989. Seismic boundary conditions for porous media, *J. geophys. Res.,* **94**(B3), 3025–3029.

Deresiewicz, H. & Skalak, R., 1963. On uniqueness in dynamic poroelasticity, *Bull. seism. Soc. Am.,* **53**(4), 783–788.

Diaz, J. & Ezziani, A., 2008. Analytical solution for wave propagation in stratified poroelastic medium. Part I: the 2D Case, *Rapport de recherché* No 6591, INRIA.

Diaz, J. & Ezziani, A., 2010. Analytical solution for wave propagation in heterogeneous acoustic/porous media. Part I: the 2D case: *Commun. Comput. Phys.,* **7**(1), 171–194.

Géli, L., Bard, P.-Y. & Schmitt, D., 1987. Seismic wave propagation in a very permeable water-saturated surface layer, *J. geophys. Res.,* **92,** 7931–7944.

Gregor, D., Moczo, P., Kristek, J., Mesgouez, A., Lefeuve-Mesgouez, G. & Kristekova, M., 2021. Subcell-resolution finite-difference modelling of seismic waves in Biot and JKD poroelastic media, *Geophys. J. Int.,* **224**(2), 760–794.

Guan, W. & Hu, H., 2011. The parameter averaging technique in finite-difference modeling of elastic waves in combined structures with solid, fluid and porous subregions, *Commun. Comput. Phys.,* **10**(3), 695–715.

Hansen, N.R., 2018. ExpoRkit code, Available at: https://github.com/nielsrhansen/expoRkit.

He, X., Yang, D., Zhou, Y., Yang, L. & Huang, X., 2021. Runge-Kutta discontinuous Galerkin method for solving wave equations in 2D isotropic and anisotropic poroelastic media at low frequencies, *Geophysics,* **86**(4), T261–T275.

He, Y., Chen, T. & Gao, J., 2020. Perfectly matched absorbing layer for modelling transient wave propagation in heterogeneous poroelastic media, *J. geophys. Eng.,* **17,** 18–34.

Iserles, A., 2009. *A First Course in the Numerical Analysis of Differential Equations,* Cambridge University Press.

Johnson, D. L., Koplik, J. & Dashen, R., 1987. Theory of dynamic permeability and tortuosity in fluid-saturated porous media, *J. Fluid Mech.,* **176,** 379–402.

Komatitsch, D. & Vilotte, J.P., 1998. The spectral-element method: an efficient tool to simulate the seismic response of 2D and 3D geological structures, *Bull. seism. Soc. Am.,* **88**(2), 368–392.

Kristek, J. & Moczo, P., 2003. Seismic-wave propagation in viscoelastic media with material discontinuities: a 3D fourth-order staggered-grid finite-difference modelling, *Bull. seism. Soc. Am.,* **93,** 2273–2280.

Kristek, J., Moczo, P., Bard, P.-Y., Hollender, F. & Stripajová, S., 2018. Computation of Amplification Factor of Earthquake Ground Motion for a Local Sedimentary Structure, *Bull. Earthquake Eng.,* **16**(6), 2451–2475

Kristek, J., Moczo, P., Chaljub, E. & Kristekova, M., 2017. An orthorhombic representation of a heterogeneous medium for the finite-difference modelling of seismic wave propagation, *Geophys. J. Int.,* **208,** 1250–1264.

Kristek, J., Moczo, P., Chaljub, E. & Kristekova, M., 2019. A discrete representation of a heterogeneous viscoelastic medium for the finite-difference modelling of seismic wave propagation, *Geophys. J. Int.,* **217,** 2021–2034.

Kristekova, M., Kristek, J. & Moczo, P. 2008. The Fortran95 program package TF_MISFIT_and_GOF_CRITERIA and User's guide at http://www.nuquake.eu/Computer_Codes/

Kristekova, M., Kristek, J. & Moczo, P., 2009. Time-frequency misfit and goodness-of-fit criteria for quantitative comparison of time signals, *Geophys. J. Int.,* **178,** 813–825.

Kristekova, M., Kristek, J., Moczo, P. & Day, S. M., 2006. Misfit criteria for quantitative comparison of seismograms, *Bull. seism. Soc. Am.,* **96,** 1836–1850.

Lähivaara, T., Ward, N.D., Huttunen, T., Koponen, J. & Kaipio, J., 2014. Estimation of aquifer dimensions from passive seismic signals with approximate wave propagation models, *Inverse Probl.,* **30,** 1–18.

Lähivaara, T., Ward, N.D., Huttunen, T., Rawlinson, Z. & Kaipio, J., 2015. Estimation of aquifer dimensions from passive seismic signals in the presence of material and source uncertainties, *Geophys. J. Int.,* **200,** 1662–1675.

Lefeuve-Mesgouez, G., Mesgouez, A., Chiavassa, G. & Lombard, B., 2012. Semi-analytical and numerical methods for computing transient waves in 2D acoustic/poroelastic stratified media. *Wave Motion,* **49**(7), 667–680.

Lovera, O.M., 1987. Boundary conditions for a fluid-saturated porous solid, *Geophysics,* **52**(2), 174–178.

Mesgouez, A. & Lefeuve-Mesgouez, G., 2009. Transient solution for multilayered poroviscoelastic media obtained by an exact stiffness matrix formulation. *Int. J. Numer. Anal. Meth. Geomech.,* **33,** 1911–1931.

Moczo, P., Gregor, D., Kristek, J. & de la Puente, J., 2019. A discrete representation of material heterogeneity for the finite-difference modelling of seismic wave propagation in a poroelastic medium, *Geophys. J. Int.,* **216**(2), 1072–1099.

Moczo, P., Kristek, J., Bard, P.-Y., Stripajová, S., Hollender, F., Chovanová, Z., Kristeková, M. & Sicilia, D., 2018. Key structural parameters affecting earthquake ground motion in 2D and 3D sedimentary structures, *Bull. Earthquake Eng.,* **16**(6), 2421–2450.

Moczo, P., Kristek, J. & Galis, M., 2014. *The Finite-Difference Modelling of Earthquake Motions: Waves and Ruptures,* Cambridge University Press.

Moczo, P., Kristek, J., Vavryčuk, V., Archuleta, R. J. & Halada, L., 2002. 3D heterogeneous staggered-grid finite-difference modeling of seismic motion with volume harmonic and arithmetic averaging of elastic moduli and densities, *Bull. seism. Soc. Am.,* **92,** 3042–3066.

Morency, C., Luo, Y. & Tromp, J., 2011. Acoustic, elastic and poroelastic simulations of CO2 sequestration crosswell monitoring based on spectral-element and adjoint methods, *Geophys. J. Int.,* **185,** 955–966.

Morency, C. & Tromp, J., 2008. Spectral-element simulations of wave propagation in porous media, *Geophys. J. Int.,* **175,** 301–345.

Ou, W. & Wang, Z., 2019. Simulation of Stoneley wave reflection from porous formation in borehole using FDTD method, *Geophys. J. Int.,* **217,** 2081–2096.

Sun, Y.-C., Hengxin, R., Zheng, X.-Z., Li, N., Zhang, W., Huang, Q. & Chen, X., 2019. 2-D poroelastic wave modelling with a topographic free surface by the curvilinear grid finite-difference method, *Geophys. J. Int.,* **218**(3), 1961–1982.

Tohti, M., Wang, Y., Xiao, W., Di, Q., Zhou, K., Wang, J., An, S. & Liao, S., 2021. Numerical simulation of seismic waves in 3D orthorhombic poroelastic medium with microseismic source implementation, *Geophys. J. Int.,* doi:10.1093/gji/ggab219.

Tomar, S. K. & Arora, A., 2006. Reflection and transmission of elastic waves at an elastic/porous solid saturated by two immiscible fluids. *Intl. J. Solids Struct.,* **43**(7-8), 1991–2013.

Ward, N.F. Dudley, Eveson, S. & Lähivaara, T., 2020. A Discontinuous Galerkin method for three-dimensional poroelastic wave propagation: forward and adjoint problems, *arXiv: 2001.09478 [physics.comp-ph].*

Ward, N.F. Dudley, Lähivaara, T. & Eveson, S., 2017. A discontinuous Galerkin method for poroelastic wave propagation: the two-dimensional case, *J. Comput. Phys.,* **350,** 690–727.

Wuttke, F., Dineva, P. & Fontara, I.-K., 2017. Influence of poroelasticity on the 3D seismic response of complex geological media, *J. Theor. Appl. Mech.,* **47**(2), 34–60.

Zhang, W., 2020. Stability analysis for wave simulation in 3D poroelastic media with the staggered-grid method, *Commun. Comput. Phys.,* **28**(2), 743–767.

Zhang, Y., Gao, J., Han, W. & He, Y., 2019. A discontinuous Galerkin method for seismic wave propagation in coupled elastic and poroelastic media, *Geophys. Prospect.,* **67,** 1392–1403.

APPENDIX A: Equations for the averaged poroelastic medium

The constitutive relations and equations of motion for the 2-D *P-SV* problem in the velocity–stress–pressure formulation for the averaged poroelastic medium may be written as (Moczo *et al.* 2019; Gregor *et al.* 2021)

$$\frac{\partial}{\partial t}\begin{bmatrix}\sigma_{xx}\\ \sigma_{zz}\\ \sigma_{xz}\\ -p\end{bmatrix} = \mathbf{S}_A \;\frac{\partial}{\partial t}\begin{bmatrix}\varepsilon_{xx}\\ \varepsilon_{zz}\\ \varepsilon_{xz}\\ \varepsilon_{w}\end{bmatrix} \tag{A1}$$

and

$$\frac{\partial}{\partial t}\begin{bmatrix}v_x\\ -q_x\\ v_z\\ -q_z\end{bmatrix} = \mathbf{R}_A \begin{bmatrix}\dfrac{\partial \sigma_{xx}}{\partial x}+\dfrac{\partial \sigma_{xz}}{\partial z}\\ \dfrac{\partial p}{\partial x}\\ P_x\\ \dfrac{\partial \sigma_{zz}}{\partial z}+\dfrac{\partial \sigma_{xz}}{\partial x}\\ \dfrac{\partial p}{\partial z}\\ P_z\end{bmatrix} \tag{A2}$$

The matrices $\mathbf{S}_A$, and $\mathbf{R}_A$ have the following forms:

$$\mathbf{S}_A \equiv \begin{bmatrix} XX + \dfrac{XP\ XP}{\Psi} & XZ + \dfrac{XP\ ZP}{\Psi} & 0 & \dfrac{XP}{\Psi} \\ XZ + \dfrac{XP\ ZP}{\Psi} & ZZ + \dfrac{ZP\ ZP}{\Psi} & 0 & \dfrac{ZP}{\Psi} \\ 0 & 0 & 2\langle\mu\rangle^{Hxz} & 0 \\ \dfrac{XP}{\Psi} & \dfrac{ZP}{\Psi} & 0 & \dfrac{1}{\Psi} \end{bmatrix} \tag{A3}$$

$$\mathbf{R}_A \equiv \left[\begin{array}{ccc:ccc} \dfrac{\langle F^x\rangle^z}{\langle S^x\rangle^z} & \dfrac{\langle G^x\rangle^z}{\langle S^x\rangle^z} & \dfrac{\langle H^x\rangle^z}{\langle S^x\rangle^z} & 0 & 0 & 0 \\ \hdashline \dfrac{\langle R^x\rangle^z\left\langle \dfrac{G^x}{R^x}\right\rangle^z}{\langle S^x\rangle^z} & \dfrac{\langle P^x\rangle^z\langle G^x\rangle^z}{\langle S^x\rangle^z} & \dfrac{\langle P^x\rangle^z\langle H^x\rangle^z}{\langle S^x\rangle^z} & 0 & 0 & 0 \\ \hdashline 0 & 0 & 0 & \dfrac{\langle F^z\rangle^x}{\langle S^z\rangle^x} & \dfrac{\langle G^z\rangle^x}{\langle S^z\rangle^x} & \dfrac{\langle H^z\rangle^x}{\langle S^z\rangle^x} \\ \hdashline 0 & 0 & 0 & \dfrac{\langle R^z\rangle^x\left\langle \dfrac{G^z}{R^z}\right\rangle^x}{\langle S^z\rangle^x} & \dfrac{\langle P^z\rangle^x\langle G^z\rangle^x}{\langle S^z\rangle^x} & \dfrac{\langle P^z\rangle^x\langle H^z\rangle^x}{\langle S^z\rangle^x} \end{array}\right] \tag{A4}$$

The above equations are valid and sufficient in case of zero or constant resistive friction. In case of the JKD frequency-dependent resistive friction, there are additional equations for the diffusive memory variables ψ_n^i; $\quad i \in \{x,\ z\}, n = 1, ..., N$:

$$\frac{\partial}{\partial t}\ \boldsymbol{\psi}^i = -\left(\mathbf{D}_A + \boldsymbol{\Omega}_A\right) \begin{bmatrix} \dfrac{\partial\,\sigma_{ij}}{\partial\,x_j} \\ \dfrac{\partial\,p}{\partial\,x_i} \\ P_i \\ q_i \\ \boldsymbol{\psi}^i \end{bmatrix} \tag{A5}$$

Here, $\boldsymbol{\psi}^i \equiv [\psi_1^i, \psi_2^i, ..., \psi_{N-1}^i, \psi_N^i]^{\mathrm{T}}$. The diffusive memory variables ψ_n^i appear in the formal wavefield variables P_x and P_z. The matrices $\mathbf{D}_A$ and $\boldsymbol{\Omega}_A$ have the following forms:

$$\mathbf{D}_A \equiv -\frac{1}{\langle S^i\rangle^s} \begin{bmatrix} \left\langle R^i\right\rangle^s\left\langle \dfrac{G^i}{R^i}\right\rangle^s & \langle P^i\rangle^s\langle G^i\rangle^s & \langle P^i\rangle^s\langle H^i\rangle^s & 0 & 0 & 0 & \cdots & 0 & 0 \\ \left\langle R^i\right\rangle^s\left\langle \dfrac{G^i}{R^i}\right\rangle^s & \langle P^i\rangle^s\langle G^i\rangle^s & \langle P^i\rangle^s\langle H^i\rangle^s & 0 & 0 & 0 & 0 & \cdots & 0 \\ \vdots & \vdots & \vdots & \vdots & \vdots & \vdots & \ddots & \vdots & \vdots \\ \left\langle R^i\right\rangle^s\left\langle \dfrac{G^i}{R^i}\right\rangle^s & \langle P^i\rangle^s\langle G^i\rangle^s & \langle P^i\rangle^s\langle H^i\rangle^s & 0 & 0 & \cdots & 0 & 0 & 0 \\ \left\langle R^i\right\rangle^s\left\langle \dfrac{G^i}{R^i}\right\rangle^s & \langle P^i\rangle^s\langle G^i\rangle^s & \langle P^i\rangle^s\langle H^i\rangle^s & 0 & 0 & 0 & \cdots & 0 & 0 \end{bmatrix} \tag{A6}$$

$$s = z \ \text{ if } \ i = x, \quad s = x \ \text{ if } \ i = z$$

and

$$\boldsymbol{\Omega}_A \equiv \begin{bmatrix} 0 & 0 & 0 & -\bar{\Omega} & \theta_1 + \bar{\Omega} & 0 & \cdots & 0 & 0 \\ 0 & 0 & 0 & -\bar{\Omega} & 0 & \theta_2 + \bar{\Omega} & 0 & \cdots & 0 \\ \vdots & \vdots & \vdots & \vdots & \vdots & \vdots & \ddots & \vdots & \vdots \\ 0 & 0 & 0 & -\bar{\Omega} & 0 & \cdots & 0 & \theta_{N-1} + \bar{\Omega} & 0 \\ 0 & 0 & 0 & -\bar{\Omega} & 0 & 0 & \cdots & 0 & \theta_N + \bar{\Omega} \end{bmatrix} \tag{A7}$$

The averaged material parameters appearing in the constitutive relations (A1) and thus in the matrix $\mathbf{S}_A$ are

$$XX = \left\langle \left\langle \Lambda - \frac{\lambda^2}{\Lambda} \right\rangle^z + \left(\left\langle \frac{\lambda}{\Lambda} \right\rangle^z \right)^2 \langle \Lambda \rangle^{Hz} \right\rangle^{Hx}$$

$$ZZ = \left\langle \left\langle \Lambda - \frac{\lambda^2}{\Lambda} \right\rangle^x + \left(\left\langle \frac{\lambda}{\Lambda} \right\rangle^x \right)^2 \langle \Lambda \rangle^{Hx} \right\rangle^{Hz}$$

$$XZ = \left\langle \frac{\lambda}{\Lambda} \right\rangle^{xz} \langle \Lambda \rangle^{Hxz} \tag{A8}$$

$$XP = \left\langle \left\langle \Lambda - \frac{\alpha\,\lambda}{\Lambda} \right\rangle^z + \left\langle \frac{\alpha}{\Lambda} \right\rangle^z \left\langle \frac{\lambda}{\Lambda} \right\rangle^z \langle \Lambda \rangle^{Hz} \right\rangle^{Hx} \times \left\langle \frac{\left\langle \alpha - \frac{\alpha\lambda}{\Lambda} \right\rangle^z + \left\langle \frac{\alpha}{\Lambda} \right\rangle^z \left\langle \frac{\lambda}{\Lambda} \right\rangle^z \langle \Lambda \rangle^{Hz}}{\left\langle \Lambda - \frac{\alpha\lambda}{\Lambda} \right\rangle^z + \left\langle \frac{\alpha}{\Lambda} \right\rangle^z \left\langle \frac{\lambda}{\Lambda} \right\rangle^z \langle \Lambda \rangle^{Hz}} \right\rangle^x \tag{A9}$$

$$ZP = \left\langle \left\langle \Lambda - \frac{\alpha\,\lambda}{\Lambda} \right\rangle^x + \left\langle \frac{\alpha}{\Lambda} \right\rangle^x \left\langle \frac{\lambda}{\Lambda} \right\rangle^x \langle \Lambda \rangle^{Hx} \right\rangle^{Hz} \times \left\langle \frac{\left\langle \alpha - \frac{\alpha\lambda}{\Lambda} \right\rangle^x + \left\langle \frac{\alpha}{\Lambda} \right\rangle^x \left\langle \frac{\lambda}{\Lambda} \right\rangle^x \langle \Lambda \rangle^{Hx}}{\left\langle \Lambda - \frac{\alpha\lambda}{\Lambda} \right\rangle^x + \left\langle \frac{\alpha}{\Lambda} \right\rangle^x \left\langle \frac{\lambda}{\Lambda} \right\rangle^x \langle \Lambda \rangle^{Hx}} \right\rangle^z \tag{A10}$$

$$\Psi = \left\langle \frac{1}{M} + \frac{\alpha^2}{\Lambda} \right\rangle^{xz} - \left(\left\langle \frac{\alpha}{\Lambda} \right\rangle^{xz} \right)^2 \langle \Lambda \rangle^{Hxz} \tag{A11}$$

The averaged material parameters appearing in the equations of motion (A2) and additional equations (A5) for the diffusive memory variables, and thus in the matrices $\mathbf{R}_A$, $\mathbf{D}_A$ and $\mathbf{\Omega}_A$ are

$$F^\xi \equiv \frac{1}{\langle \rho_f \rangle^\xi} \quad G^\xi \equiv \frac{1}{\langle m \rangle^\xi} \quad H^\xi \equiv \frac{\langle B \rangle^\xi}{\langle m \rangle^\xi}$$

$$P^\xi \equiv \frac{\langle \rho \rangle^\xi}{\langle \rho_f \rangle^\xi} \quad Q^\xi \equiv \frac{\langle \rho_f \rangle^\xi}{\langle m \rangle^\xi} \quad R^\xi \equiv \left\langle \frac{1}{\rho_f} \right\rangle^\xi$$

$$S^\xi \equiv \langle P^\xi \rangle - \langle Q^\xi \rangle \tag{A12}$$

and

$$\bar{\Omega} \equiv \left(\frac{n_J}{4} \right)^2 \left\{ \frac{1}{2} \left[\langle H^x \rangle^z + \langle H^z \rangle^x \right] \right\}^2 \tag{A13}$$

Symbols $\langle \Phi \rangle^\xi$ and $\langle \Phi \rangle^{H\xi}$ indicate arithmetic and harmonic averages of Φ, respectively, in the ξ-direction. Symbols $\langle \Phi \rangle^{\xi\upsilon}$ and $\langle \Phi \rangle^{H\xi\upsilon}$ indicate arithmetic and harmonic averages of Φ, respectively, in the ξ-direction and then in the υ-direction. In general, the averaging applies to a representative area centred at a grid position of a relevant field variable.

If we consider solving the equations for the averaged medium using a staggered-grid FD scheme, then the averaging applies to an area of a grid cell $h \times h$ centred at a position of the corresponding stress component or pore pressure or particle-velocity component. In case of a generally heterogeneous medium, the averages are evaluated by a numerical integration. Fig. A1 shows the staggered FD grid cell with indications of grid positions of the averaged material parameters appearing in relations (A3)–(A13).

APPENDIX B: Matrices for the unifying equation

Matrices appearing in eqs (30) and (32):

X_{pq}, Z_{pq} are the $p \times q = (2N + 8) \times (2N + 8)$ matrices

$$X_{pq} \equiv \begin{pmatrix} 0_{N+2,\,N+2} & 0_{N+2,\,N+2} & X^{(1)}_{N+2,\,4} \\ 0_{N+2,\,N+2} & 0_{N+2,\,N+2} & X^{(2)}_{N+2,\,4} \\ X^{(3)}_{4,\,N+2} & X^{(4)}_{4,\,N+2} & 0_{4,\,4} \end{pmatrix} \tag{B1}$$

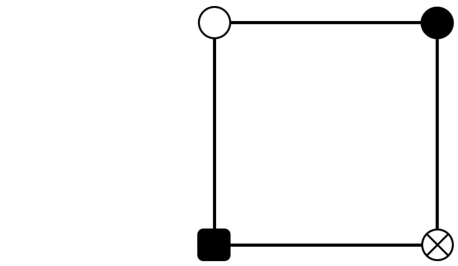

$\bigcirc$ σ_{zx}^{m}

$2\langle\mu\rangle^{Hxz}$

$\bullet$ $v_x^{m+1/2},\ q_x^{m+1/2},\ \psi_n^{x;\,m+1/2}$

$\left\langle F^x\right\rangle^z, \left\langle G^x\right\rangle^z, \left\langle H^x\right\rangle^z, \left\langle P^x\right\rangle^z, \left\langle R^x\right\rangle^z, \left\langle S^x\right\rangle^z$

$\blacksquare$ $v_z^{m+1/2},\ q_z^{m+1/2},\ \psi_n^{z;\,m+1/2}$

$\left\langle F^z\right\rangle^x, \left\langle G^z\right\rangle^x, \left\langle H^z\right\rangle^x, \left\langle P^z\right\rangle^x, \left\langle R^z\right\rangle^x, \left\langle S^z\right\rangle^x$

$\otimes$ $\sigma_{xx}^{m},\ \sigma_{zz}^{m}, p^m$

XX, ZZ, XZ, XP, ZP, Ψ

Figure A1. Positions of the field variables (discrete approximations of the true variables in the continuum) and averaged material parameters in the staggered FD grid.

$$X_{N+2,\,4}^{(1)} \equiv \begin{pmatrix} -\dfrac{\langle F^x\rangle^z}{\langle S^x\rangle^z} & 0 & 0 & -\dfrac{\langle G^x\rangle^z}{\langle S^x\rangle^z} \\ \dfrac{\langle R^x\rangle^z\left\langle \dfrac{G^x}{R^x}\right\rangle^z}{\langle S^x\rangle^z} & 0 & 0 & \dfrac{\langle P^x\rangle^z\langle G^x\rangle^z}{\langle S^x\rangle^z} \\ \dfrac{\langle R^x\rangle^z\left\langle \dfrac{G^x}{R^x}\right\rangle^z}{\langle S^x\rangle^z} & 0 & 0 & \dfrac{\langle P^x\rangle^z\langle G^x\rangle^z}{\langle S^x\rangle^z} \\ \vdots & \vdots & \vdots & \vdots \\ \dfrac{\langle R^x\rangle^z\left\langle \dfrac{G^x}{R^x}\right\rangle^z}{\langle S^x\rangle^z} & 0 & 0 & \dfrac{\langle P^x\rangle^z\langle G^x\rangle^z}{\langle S^x\rangle^z} \end{pmatrix} \tag{B2}$$

$$X_{N+2,\,4}^{(2)} \equiv \begin{pmatrix} 0 & -\dfrac{\langle F^z\rangle^x}{\langle S^z\rangle^x} & 0 & 0 \\ 0 & \dfrac{\langle R^z\rangle^x\left\langle \dfrac{G^z}{R^z}\right\rangle^x}{\langle S^z\rangle^x} & 0 & 0 \\ 0 & \dfrac{\langle R^z\rangle^x\left\langle \dfrac{G^z}{R^z}\right\rangle^x}{\langle S^z\rangle^x} & 0 & 0 \\ \vdots & \vdots & \vdots & \vdots \\ 0 & \dfrac{\langle R^z\rangle^x\left\langle \dfrac{G^z}{R^z}\right\rangle^x}{\langle S^z\rangle^x} & 0 & 0 \end{pmatrix} \tag{B3}$$

$$X^{(3)}_{4,\,N+2} \equiv \begin{pmatrix} -XX & 0 & 0 & \cdots & 0 \\ 0 & 0 & 0 & \cdots & 0 \\ -XZ & 0 & 0 & \cdots & 0 \\ \dfrac{XP}{\Psi} & \dfrac{1}{\Psi} & 0 & \cdots & 0 \end{pmatrix}, \quad X^{(4)}_{4,\,N+2} \equiv \begin{pmatrix} 0 & 0 & 0 & \cdots & 0 \\ -\langle\mu\rangle^{Hxz} & 0 & 0 & \cdots & 0 \\ 0 & 0 & 0 & \cdots & 0 \\ 0 & 0 & 0 & \cdots & 0 \end{pmatrix} \tag{B4}$$

$$Z_{pq} \equiv \begin{pmatrix} 0_{N+2,\,N+2} & 0_{N+2,\,N+2} & Z^{(1)}_{N+2,\,4} \\ 0_{N+2,\,N+2} & 0_{N+2,\,N+2} & Z^{(2)}_{N+2,\,4} \\ Z^{(4)}_{4,\,N+2} & Z^{(4)}_{4,\,N+2} & 0_{4,\,4} \end{pmatrix} \tag{B5}$$

$$X^{(1)}_{N+2,\,4} \equiv \begin{pmatrix} 0 & -\dfrac{\langle F^x\rangle^z}{\langle S^x\rangle^z} & 0 & 0 \\ 0 & \dfrac{\langle R^x\rangle^z\left\langle \dfrac{G^x}{R^x}\right\rangle^z}{\langle S^x\rangle^z} & 0 & 0 \\ 0 & \dfrac{\langle R^x\rangle^z\left\langle \dfrac{G^x}{R^x}\right\rangle^z}{\langle S^x\rangle^z} & 0 & 0 \\ \vdots & \vdots & \vdots & \vdots \\ 0 & \dfrac{\langle R^x\rangle^z\left\langle \dfrac{G^x}{R^x}\right\rangle^z}{\langle S^x\rangle^z} & 0 & 0 \end{pmatrix} \tag{B6}$$

$$X^{(2)}_{N+2,\,4} \equiv \begin{pmatrix} 0 & 0 & -\dfrac{\langle F^z\rangle^x}{\langle S^z\rangle^x} & -\dfrac{\langle G^z\rangle^x}{\langle S^z\rangle^x} \\ 0 & 0 & \dfrac{\langle R^z\rangle^x\left\langle \dfrac{G^z}{R^z}\right\rangle^x}{\langle S^z\rangle^x} & \dfrac{\langle P^z\rangle^x\langle G^z\rangle^x}{\langle S^z\rangle^x} \\ 0 & 0 & \dfrac{\langle R^z\rangle^x\left\langle \dfrac{G^z}{R^z}\right\rangle^x}{\langle S^z\rangle^x} & \dfrac{\langle P^z\rangle^x\langle G^z\rangle^x}{\langle S^z\rangle^x} \\ \vdots & \vdots & \vdots & \vdots \\ 0 & 0 & \dfrac{\langle R^z\rangle^x\left\langle \dfrac{G^z}{R^z}\right\rangle^x}{\langle S^z\rangle^x} & \dfrac{\langle P^z\rangle^x\langle G^z\rangle^x}{\langle S^z\rangle^x} \end{pmatrix} \tag{B7}$$

$$Z^{(3)}_{4,\,N+2} \equiv X^{(4)}_{4,\,N+2}, \quad Z^{(4)}_{4,\,N+2} \equiv \begin{pmatrix} -XZ & 0 & 0 & \cdots & 0 \\ 0 & 0 & 0 & \cdots & 0 \\ -ZZ & 0 & 0 & \cdots & 0 \\ \dfrac{ZP}{\Psi} & \dfrac{1}{\Psi} & 0 & \cdots & 0 \end{pmatrix} \tag{B8}$$

$$T_{pq} \equiv \begin{pmatrix} 1_{N+2,\,N+2} & 0_{N+2,\,N+2} & 0_{N+2,\,4} \\ 0_{N+2,\,N+2} & 1_{N+2,\,N+2} & 0_{N+2,\,4} \\ 0_{4,\,N+2} & 0_{4,\,N+2} & T^{(1)}_{4,\,4} \end{pmatrix} \tag{B9}$$

$$T^{(1)}_{4,\,4} \equiv \begin{pmatrix} 1 & 0 & 0 & XP \\ 0 & 1 & 0 & 0 \\ 0 & 0 & 1 & ZP \\ 0 & 0 & 0 & 1 \end{pmatrix} \tag{B10}$$

S_{pq} is the $p \times q = (2N + 8) \times (2N + 8)$ matrix

$$S_{pq} \equiv \begin{pmatrix} S^x_{N+2,\,N+2} & 0_{N+2,\,N+2} & 0_{N+2,\,4} \\ 0_{N+2,\,N+2} & S^z_{N+2,\,N+2} & 0_{N+2,\,4} \\ 0_{4,\,N+2} & 0_{4,\,N+2} & 0_{4,\,4} \end{pmatrix} \tag{B11}$$

$$S^x_{N+2,\,N+2} \equiv \begin{pmatrix} 0 & 0 & -\frac{\langle H^x\rangle^z}{\langle S^x\rangle^z}a_1 & \cdots & -\frac{\langle H^x\rangle^z}{\langle S^x\rangle^z}a_N \\ 0 & 0 & \frac{\langle P^x\rangle^z\langle H^x\rangle^z}{\langle S^x\rangle^z}a_1 & \cdots & \frac{\langle P^x\rangle^z\langle H^x\rangle^z}{\langle S^x\rangle^z}a_N \\ 0 & -\bar{\Omega} & \frac{\langle P^x\rangle^z\langle H^x\rangle^z}{\langle S^x\rangle^z}a_1 + (\theta_1+\bar{\Omega}) & \cdots & \frac{\langle P^x\rangle^z\langle H^x\rangle^z}{\langle S^x\rangle^z}a_N \\ \vdots & \vdots & \vdots & \cdots & \vdots \\ 0 & -\bar{\Omega} & \frac{\langle P^x\rangle^z\langle H^x\rangle^z}{\langle S^x\rangle^z}a_1 & \cdots & \frac{\langle P^x\rangle^z\langle H^x\rangle^z}{\langle S^x\rangle^z}a_N + (\theta_N+\bar{\Omega}) \end{pmatrix} \tag{B12}$$

$$S^z_{N+2,\,N+2} \equiv \begin{pmatrix} 0 & 0 & -\frac{\langle H^z\rangle^x}{\langle S^z\rangle^x}a_1 & \cdots & -\frac{\langle H^z\rangle^x}{\langle S^z\rangle^x}a_N \\ 0 & 0 & \frac{\langle P^z\rangle^x\langle H^z\rangle^x}{\langle S^z\rangle^x}a_1 & \cdots & \frac{\langle P^z\rangle^x\langle H^z\rangle^x}{\langle S^z\rangle^x}a_N \\ 0 & -\bar{\Omega} & \frac{\langle P^z\rangle^x\langle H^z\rangle^x}{\langle S^z\rangle^x}a_1 + (\theta_1+\bar{\Omega}) & \cdots & \frac{\langle P^z\rangle^x\langle H^z\rangle^x}{\langle S^z\rangle^x}a_N \\ \vdots & \vdots & \vdots & \cdots & \vdots \\ 0 & -\bar{\Omega} & \frac{\langle P^z\rangle^x\langle H^z\rangle^x}{\langle S^z\rangle^x}a_1 & \cdots & \frac{\langle P^z\rangle^x\langle H^z\rangle^x}{\langle S^z\rangle^x}a_N + (\theta_N+\bar{\Omega}) \end{pmatrix} \tag{B13}$$

The abscissae $\theta_1, \ldots \theta_N$ are the same for the whole averaged model, whereas weights $a_1, \ldots a_N$ are calculated for each grid cell in the averaged model.

APPENDIX C: Simplified matrices

Application of relation (19) significantly simplifies matrices $S^i_{N+2,\,N+2};\ \ i \in \{x,\ z\}$:

$$S^x_{N+2,\,N+2} = S^z_{N+2,\,N+2} = \begin{pmatrix} 0 & 0 & 0 & \cdots & 0 \\ 0 & 0 & 0 & \cdots & 0 \\ 0 & 0 & \theta_1 & \cdots & 0 \\ \vdots & \vdots & \vdots & \cdots & \vdots \\ 0 & 0 & 0 & \cdots & \theta_N \end{pmatrix} \tag{C1}$$

Since the matrices are diagonal, the matrix exponentials $\exp(-S^x\,\Delta)$ and $\exp(-S^z\,\Delta)$ can be obtained by exponentiating each entry on the diagonal

$$E \equiv \exp\left(-S^i_{N+2,\,N+2}\,\Delta\right) \approx \tilde{S}^{ti}_{N+2,\,N+2} = \begin{pmatrix} 1 & 0 & 0 & \cdots & 0 \\ 0 & 1 & 0 & \cdots & 0 \\ 0 & 0 & e^{-\theta_1\,\Delta} & \cdots & 0 \\ \vdots & \vdots & \vdots & \cdots & \vdots \\ 0 & 0 & 0 & \cdots & e^{-\theta_N\,\Delta} \end{pmatrix};\ \ i \in \{x,\ z\} \tag{C2}$$

Then, the analytical field variables ${}^i\vec{Q}^*|^{m+1/2};\ \ i \in \{x, z\}$ can be calculated as

$${}^i\vec{Q}^*\Big|^{m+1/2} = E\,{}^i\vec{Q}\Big|^{m-1/2};\ \ i \in \{x, z\} \tag{C3}$$

APPENDIX D: The FD scheme

The FD scheme for updating field variables VX, QX, TXZ, FP and ψ^x_l. Schemes for updating field variables VZ, QZ, TXX, TZZ and ψ^z_l are analogous. All they can be found in the paper by Gregor *et al.* (2021).

Let VX, VZ and QX, QZ be discrete grid values of v_x, v_z and q_x, q_z, respectively. Let TXX, TZZ, TXZ and FP be discrete grid values of σ_{xx}, σ_{zz}, σ_{xz} and fluid pressure p, respectively. For the grid values of the material parameters, we will use symbols defined by eqs (A8)–(A11) and (A12). Fig. A1 shows positions of the field variables and material parameters in the grid cell. For brevity, we indicate material parameters as they appear in the equations for the smoothly heterogeneous medium. Denote the fourth-order accurate operators of

the first spatial derivatives with respect to x and z coordinates:

$$D_x^{(4)}\,\Phi^n_{I,L} \equiv \frac{1}{h}\left[\tfrac{9}{8}\left(\Phi^n_{I+1/2,\,L}-\Phi^n_{I-1/2,\,L}\right)-\tfrac{1}{24}\left(\Phi^n_{I+3/2,\,L}-\Phi^n_{I-3/2,\,L}\right)\right]$$
$$D_z^{(4)}\,\Phi^n_{I,L} \equiv \frac{1}{h}\left[\tfrac{9}{8}\left(\Phi^n_{I,\,L+1/2}-\Phi^n_{I,\,L-1/2}\right)-\tfrac{1}{24}\left(\Phi^n_{I,\,L+3/2}-\Phi^n_{I,\,L-3/2}\right)\right] \tag{D1}$$

The FD scheme consists of explicit FD formulae for updating the solid and fluid particle-velocity components, diffusive memory variables, stress components and fluid pressure:

$$\begin{aligned}
VX^{m+1/2}_{I,\,L+1/2} &= VX^{*}_{I,\,L+1/2}\\
&\quad+\frac{1}{\langle S^x\rangle^z_{I,\,L+1/2}}\frac{\Delta}{h}\left\{\langle F^x\rangle^z_{I,\,L+1/2}\left[D_x^{(4)}\,TXX^m_{I,\,L+1/2}+D_z^{(4)}\,TXZ^m_{I,\,L+1/2}\right]\right.\\
&\quad\left.+\,\langle G^x\rangle^z_{I,\,L+1/2}\,D_x^{(4)}\,FP^m_{I,\,L+1/2}\right\}\\
VX^{*}_{I,\,L+1/2} &= \tilde{s}^{v_x}_{v_x;I,\,L+1/2}\,VX^{m-1/2}_{I,\,L+1/2}+\tilde{s}^{q_x}_{v_x;I,\,L+1/2}\,QX^{m-1/2}_{I,\,L+1/2}\\
&\quad+\tilde{s}^{\psi^x_1}_{v_x;I,\,L+1/2}\,\psi^{x;\,m-1/2}_{1;\,I,\,L+1/2}+\ldots+\tilde{s}^{\psi^x_N}_{v_x;I,\,L+1/2}\,\psi^{x;\,m-1/2}_{N;\,I,\,L+1/2}
\end{aligned} \tag{D2}$$

$$\begin{aligned}
QX^{m+1/2}_{I,\,L+1/2} &= QX^{*}_{I,\,L+1/2}\\
&\quad-\frac{1}{\langle S^x\rangle^z_{I,\,L+1/2}}\frac{\Delta}{h}\left\{\left(\langle R^x\rangle^z\left\langle\frac{G^x}{R^x}\right\rangle^z\right)_{I,\,L+1/2}\left[D_x^{(4)}\,TXX^m_{I,\,L+1/2}+D_z^{(4)}\,TXZ^m_{I,\,L+1/2}\right]\right.\\
&\quad\left.+\left(\langle P^x\rangle^z\langle G^x\rangle^z\right)_{I,\,L+1/2}D_x^{(4)}\,FP^m_{I,\,L+1/2}\right\}\\
QX^{*}_{I,\,L+1/2} &= \tilde{s}^{v_x}_{q_x;I,\,L+1/2}\,VX^{m-1/2}_{I,\,L+1/2}+\tilde{s}^{q_x}_{q_x;I,\,L+1/2}\,QX^{m-1/2}_{I,\,L+1/2}\\
&\quad+\tilde{s}^{\psi^x_1}_{q_x;I,\,L+1/2}\,\psi^{x;\,m-1/2}_{1;\,I,\,L+1/2}+\ldots+\tilde{s}^{\psi^x_N}_{q_x;I,\,L+1/2}\,\psi^{x;\,m-1/2}_{N;\,I,\,L+1/2}
\end{aligned} \tag{D3}$$

$$\begin{aligned}
\psi^{x;m+1/2}_{n;I,\,L+1/2} &= \psi^{x*}_{n;I,\,L+1/2}\\
&\quad-\frac{1}{\langle S^x\rangle^z_{I,\,L+1/2}}\frac{\Delta}{h}\left\{\left(\langle R^x\rangle^z\left\langle\frac{G^x}{R^x}\right\rangle^z\right)_{I,\,L+1/2}\left[D_x^{(4)}\,TXX^m_{I,\,L+1/2}+D_z^{(4)}\,TXZ^m_{I,\,L+1/2}\right]\right.\\
&\quad\left.+\left(\langle P^x\rangle^z\langle G^x\rangle^z\right)_{I,\,L+1/2}D_x^{(4)}\,FP^m_{I,\,L+1/2}\right\}\\
\psi^{x*}_{n;I,\,L+1/2} &= \tilde{s}^{v_x}_{\psi^x_n;I,\,L+1/2}\,VX^{m-1/2}_{I,\,L+1/2}+\tilde{s}^{q_x}_{\psi^x_n;I,\,L+1/2}\,QX^{m-1/2}_{I,\,L+1/2}\\
&\quad+\tilde{s}^{\psi^x_1}_{\psi^x_n;I,\,L+1/2}\,\psi^{x;\,m-1/2}_{1;\,I,\,L+1/2}+\ldots+\tilde{s}^{\psi^x_N}_{\psi^x_n;I,\,L+1/2}\,\psi^{x;\,m-1/2}_{N;\,I,\,L+1/2}\\
n &= 1,\ldots,\ N
\end{aligned} \tag{D4}$$

$$\begin{aligned}
TXZ^m_{I,\,L+1} &= TXZ^{m-1}_{I,\,L+1}\\
&\quad+\frac{\Delta}{h}\frac{\langle\mu\rangle^{Hxz}_{I,\,L+1}}{2}\left[D_z^{(4)}VX^{m-1/2}_{I+1/2,\,L+1/2}+D_x^{(4)}VZ^{m-1/2}_{I+1/2,\,L+1/2}\right]
\end{aligned} \tag{D5}$$

$$\begin{aligned}
FP^m_{I+1/2,\,L+1/2} &= FP^{m-1}_{I+1/2,\,L+1/2}\\
&\quad-\frac{\Delta}{h}\left\{\left(\frac{XP}{\Psi}\right)_{I+1/2,\,L+1/2}D_x^{(4)}VX^{m-1/2}_{I+1/2,\,L+1/2}\right.\\
&\quad+\left(\frac{ZP}{\Psi}\right)_{I+1/2,\,L+1/2}D_z^{(4)}VZ^{m-1/2}_{I+1/2,\,L+1/2}\\
&\quad+\left(\frac{1}{\Psi}\right)_{I+1/2,\,L+1/2}D_x^{(4)}QX^{m-1/2}_{I+1/2,\,L+1/2}\\
&\quad\left.+\left(\frac{1}{\Psi}\right)_{I+1/2,\,L+1/2}D_z^{(4)}QZ^{m-1/2}_{I+1/2,\,L+1/2}\right\}
\end{aligned} \tag{D6}$$

The FD formulae for the remaining field components are specified in Appendix B of the paper by Gregor *et al.* (2021).

In case of the non-zero constant resistive friction, $b = \text{const} > 0$, eq. (D4) disappear and the second equations in (D2) and (D3) simplify:

$$VX^{*}_{I,\,L+1/2} = VX^{m-1/2}_{I,\,L+1/2}+\frac{1}{\langle P^x\rangle^z_{I,\,L+1/2}}\left[1-\exp\left(-\Delta\ PHS_{I,\,L+1/2}\right)\right]QX^{m-1/2}_{I,\,L+1/2} \tag{D7}$$

$$QX^{*}_{I,\,L+1/2} = \exp\left(-\Delta\ PHS_{I,\,L+1/2}\right)QX^{m-1/2}_{I,\,L+1/2} \tag{D8}$$

with $PHS \equiv \langle P^x\rangle^z\langle H^x\rangle^z/\langle S^x\rangle^z$.